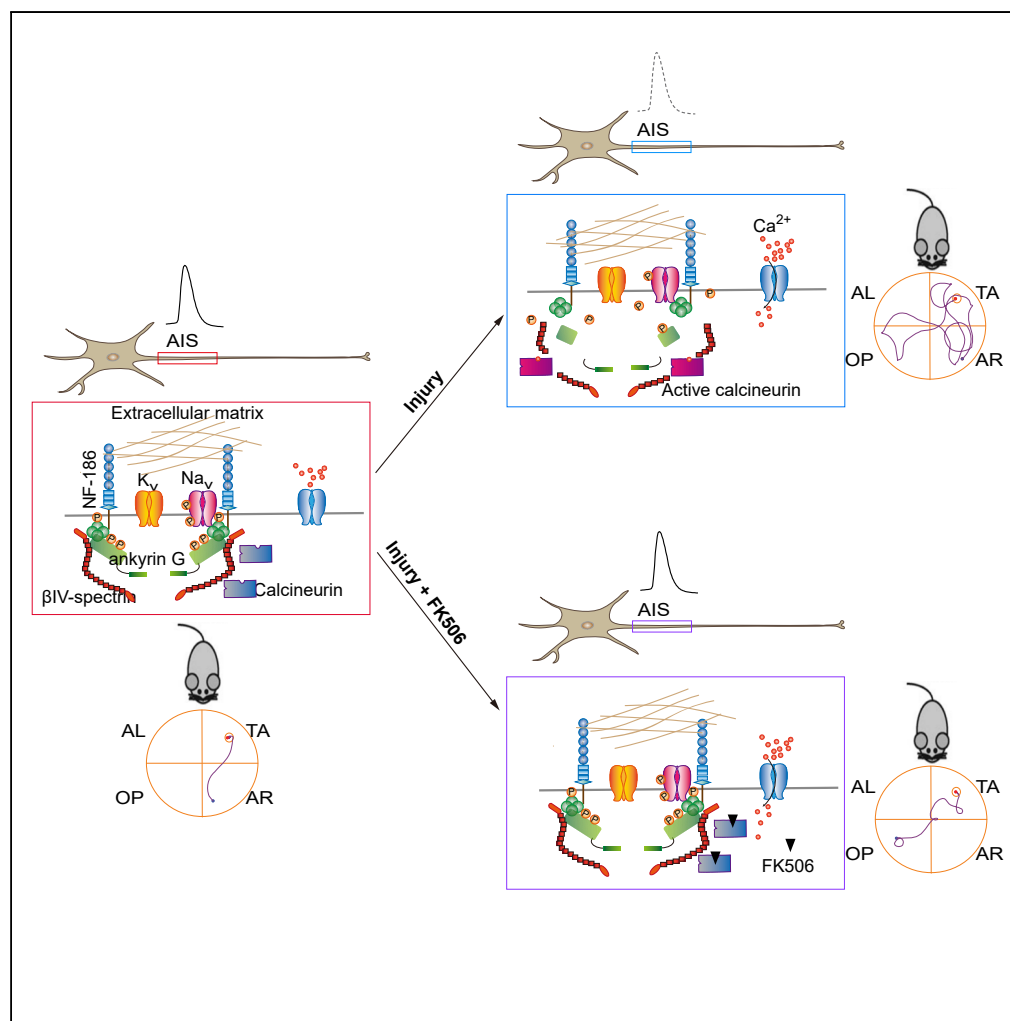## Article

Calcineurin Signaling Mediates Disruption of the Axon Initial Segment Cytoskeleton after Injury

Yanan Zhao,
Xuanyuan Wu, Xin
Chen, ..., Cheng
Xiao, Guisheng
Zhong, Shuijin He

zhongsh@shanghaitech.edu.
cn (G.Z.)
heshj@shanghaitech.edu.cn
(S.H.)

HIGHLIGHTS

Ion channels are mostly
retained at the AIS after
ischemic injury

Neurofascin is required for
clustering ion channels at
the AIS after ischemia

Calcineurin inhibition
protects AIS structural
integrity and function
from ischemia

Calcineurin inhibition
protects cognitive
function against
impairment by ischemia

Article

Calcineurin Signaling Mediates Disruption of the Axon Initial Segment Cytoskeleton after Injury

Yanan Zhao,[1,6] Xuanyuan Wu,[1,6] Xin Chen,[1] Jianan Li,[1] Cuiping Tian,[2] Jiangrui Chen,[1,3,4] Cheng Xiao,[5] Guisheng Zhong,[1,2,*] and Shuijin He[1,7,*]

SUMMARY

The axon initial segment (AIS) cytoskeleton undergoes rapid and irreversible disruption prior to cell death after injury, and loss of AIS integrity can produce profound neurological effects on the nervous system. Here we described a previously unrecognized mechanism for ischemia-induced alterations in AIS integrity. We show that in hippocampal CA1 pyramidal neurons $Na_v1.6$ mostly preserves at the AIS after disruption of the cytoskeleton in a mouse model of middle cerebral artery occlusion. Genetic removal of neurofascin-186 leads to rapid disruption of $Na_v1.6$ following injury, indicating that neurofascin is required for $Na_v1.6$ maintenance at the AIS after cytoskeleton collapse. Importantly, calcineurin inhibition with FK506 fully protects AIS integrity and sufficiently prevents impairments of spatial learning and memory from injury. This study provides evidence that calcineurin activation is primarily involved in initiating disassembly of the AIS cytoskeleton and that maintaining AIS integrity is crucial for therapeutic strategies to facilitate recovery from injury.

INTRODUCTION

The axon initial segment (AIS) is a specialized ~30-μm long proximal axon that contains ~30- to 50-fold higher density of voltage-gated sodium channels (Na_v) than the soma and dendrites (Kole et al., 2008). Owing to its unique property, the AIS is pivotal for generating an action potential in response to the integration of synaptic inputs under physiological conditions. Within the AIS subdomain, the cytoskeletal proteins including Ankyrin G (AnkG) and βIV-spectrin, together with neurofascin (Nfasc) and neuronal cell adhesion molecule (NrCAM), assemble Na_v and voltage-gated potassium channels (K_v) to build an exquisite hierarchical structure. AnkG serves as an AIS master organizer to recruit Na_v to the AIS during development and then βIV-spectrin tethers the AnkG-Na_v complex to the axonal actin. In contrast, Nfasc is not required for AIS assembly and does not directly interact with channel-forming α subunits of Na_v. Instead, Nfasc stabilizes the AIS by directly interacting with the extracellular matrix (Hedstrom et al., 2007; Ratcliffe et al., 2001; Zonta et al., 2011). It is interesting to know whether Nfasc is capable of stabilizing Na_v at the AIS in the absence of AnkG under pathological conditions.

The AIS is very vulnerable to damage under pathophysiological conditions. For example, the AIS cytoskeleton is rapidly disrupted prior to cell death following medial cerebral artery occlusion (MCAO) in the peri-infarct and infarction core regions of the rodent brain (Hinman et al., 2013; Schafer et al., 2009). Inhibition of calpain only attenuates disruption of the AIS cytoskeleton in response to injury *in vitro* and *in vivo*, implicating that the AIS cytoskeletal proteins are proteolyzed partially through activation of the Ca^{2+}-dependent calpain. However, inhibition of calcineurin with FK506 efficiently protects against cell deaths induced by ischemia in a mouse model of MCAO (Sharkey and Butcher, 1994). Moreover, blockade of calcineurin prevents activity-dependent AIS plasticity in cultured hippocampal neurons (Evans et al., 2013). These raise the question as to whether calcineurin is involved in regulating rapid AIS disruption under pathological conditions.

In the present study, we investigated the peri-infarct regions because axonal sprouting and synaptic reorganization in these regions are essential for recovery of human patients from neurological injury (Nudo, 2013; Wieloch and Nikolich, 2006). Given the critical role of the AIS in synaptic transmission, protection of the AIS in these regions after injury might be the first step to be considered for patient recovery. We thus began to compare the susceptibilities of the peri-infarct regions to ischemia using a commonly

[1]School of Life Science and Technology, ShanghaiTech University, 393 Middle Huaxia Road, Pudong New District, Shanghai 201210, China

[2]iHuman Institute, ShanghaiTech University, 393 Middle Huaxia Road, Pudong New District, Shanghai 201210, China

[3]Institute of Neuroscience, Shanghai Institutes for Biological Sciences, Chinese Academy of Sciences, Shanghai, China

[4]University of Chinese Academy of Sciences, Beijing, China

[5]School of Anesthesiology, Xuzhou Medical University, 209 Tongshan Road, KJL-D423, Xuzhou, Jiangsu Province 221004, China

[6]These authors contributed equally

[7]Lead Contact

*Correspondence: zhongsh@shanghaitech.edu.cn (G.Z.), heshj@shanghaitech.edu.cn (S.H.)

employed animal model of stroke MCAO that represents focal brain ischemia in human patients. We found that the AIS cytoskeleton was completely disrupted after 2 h of MCAO in hippocampal CA1 pyramidal neurons but not in the somatosensory cortex or striatum. In contrast, Nfasc and $Na_v1.6$ were yet retained at the AIS after 4–6 h of MCAO. Genetic ablation of Nfasc promoted disruption of $Na_v1.6$ at the AIS following injury, suggesting a critical role of Nfasc in the retention of $Na_v1.6$ under pathophysiological conditions. Importantly, administration of a calcineurin inhibitor FK506 immediately after MCAO surgery completely prevented AnkG disruption, and impairments of AP generation, AP-dependent synaptic transmission, and spatial learning and memory resulting from ischemic injury.

RESULTS

### The Hippocampal AIS Cytoskeleton Is Preferentially Susceptible to Injury

To determine the vulnerability of the AIS to injury in different peri-infarct brain regions, mice were subjected to MCAO for various times by MCA thread insertion. The severity of AIS damage was examined by immunofluorescence (IF) staining of the scaffold protein AnkG in three peri-infarct regions: the somatosensory cortex, the hippocampus, and the thalamus (Figure 1A) (Popp et al., 2009). Compared with the uninjured (contralateral) side of the brain, the intensity and the length of AnkG staining were slightly reduced in the three regions of the injured side (ipsilateral) following 1 h of MCAO. As the occlusion time went longer, more than 50% of AnkG was preserved in the ipsilateral somatosensory cortex (SCC) after 6 h of MCAO, whereas AnkG was retained in the ipsilateral thalamus within 4 h of MCAO but absent at 6 h after the onset of occlusion (Figures 1B–1D). In contrast, AnkG was undetectable in the ipsilateral hippocampal CA1 region after 2 h of MCAO (Figures 1B–1D). Analogous results were observed in the hippocampal CA3 and DG regions (Figure S1). We next focused our further mechanical study on the hippocampus. Similar to AnkG, the AIS cytoskeletal protein βIV-spectrin was no longer observed at the AIS of ipsilateral hippocampal CA1 pyramidal cells after 2 h of MCAO (Figures S2A and S2B).

To confirm these immunostaining results, we performed immunoblot analyses of hippocampal homogenates from sham or MCAO mice with antibodies against the C-terminal or spectrin-binding domains of AnkG. Immunoblots with both antibodies revealed a significant reduction in the amount of full-length AnkG in the contralateral compared with the ipsilateral after 1 h of MCAO. The full-length AnkG was rarely detected in the ipsilateral hippocampus with antibodies either against the C-terminal domain (Figures 1E and 1F) or against the spectrin-binding domain of AnkG after 2 h of MCAO (Figures S2C and S2D). Notably, no breakdown products of AnkG were detected in ipsilateral hippocampi after injury. Disruption of AnkG was not a consequence of cell death because we only observed a few TUNEL-positive cells in the hippocampus at this time point (Figure S1), consistent with the notion that cell death and AIS disruption are two independent events (Schafer et al., 2009). Collectively, these results suggest that the hippocampal AIS cytoskeleton is preferentially susceptible to injury.

Sodium Channels at the AIS Are Resistant to Injury-Induced Disruption

AnkG is required for assembly of Na_v channel clustering at the AIS where action potentials are initiated (Hedstrom et al., 2007; Jenkins and Bennett, 2001; Kole et al., 2008; Zhou et al., 1998). To examine whether AnkG disruption led to disassembly of Na_v, we performed IF staining of a Na_v subtype $Na_v1.6$ that is predominantly expressed in the hippocampal AIS. Unlike AnkG, the intensity and length of $Na_v1.6$ at the AIS were not significantly reduced following 2 h of MCAO (Figures 2A–2C), but only the intensity was decreased by ~26% at the 4-h time point (Figure 2C). Analogous results were observed for another AIS voltage-gated ion channel $K_v7.2$ (Figures S3A and S3B). To further examine whether nanoscale organizations of the AIS cytoskeleton and anchored ion channels were altered after injury, we performed super-resolution simulated emission depleted (STED) imaging to analyze the distribution of βIV-spectrin and $Na_v1.6$ at the AIS. We found that $Na_v1.6$ and βIV-spectrin showed periodic arrangements in the ipsilateral AIS comparable to the contralateral after 1 h of MCAO (Figures 2D and S3C). The periodic pattern of $Na_v1.6$ was slightly altered after 2 h of MCAO when the AIS cytoskeleton was depleted (Figure 2D).

Previous studies showed that Na_v was subject to proteolysis after injury (Czogalla and Sikorski, 2005; Schafer et al., 2009; White et al., 2000). To examine the possibility that $Na_v1.6$ might be broken down into fragments after injury, we performed immunoblot analyses of hippocampal homogenates with antibodies against $Na_v1.6$. In the ipsilateral hippocampus, we identified low-molecular-weight fragments with ~82 kD and ~90 kD from $Na_v1.6$. These bands showed up at the 1-h time point, and their density was increased
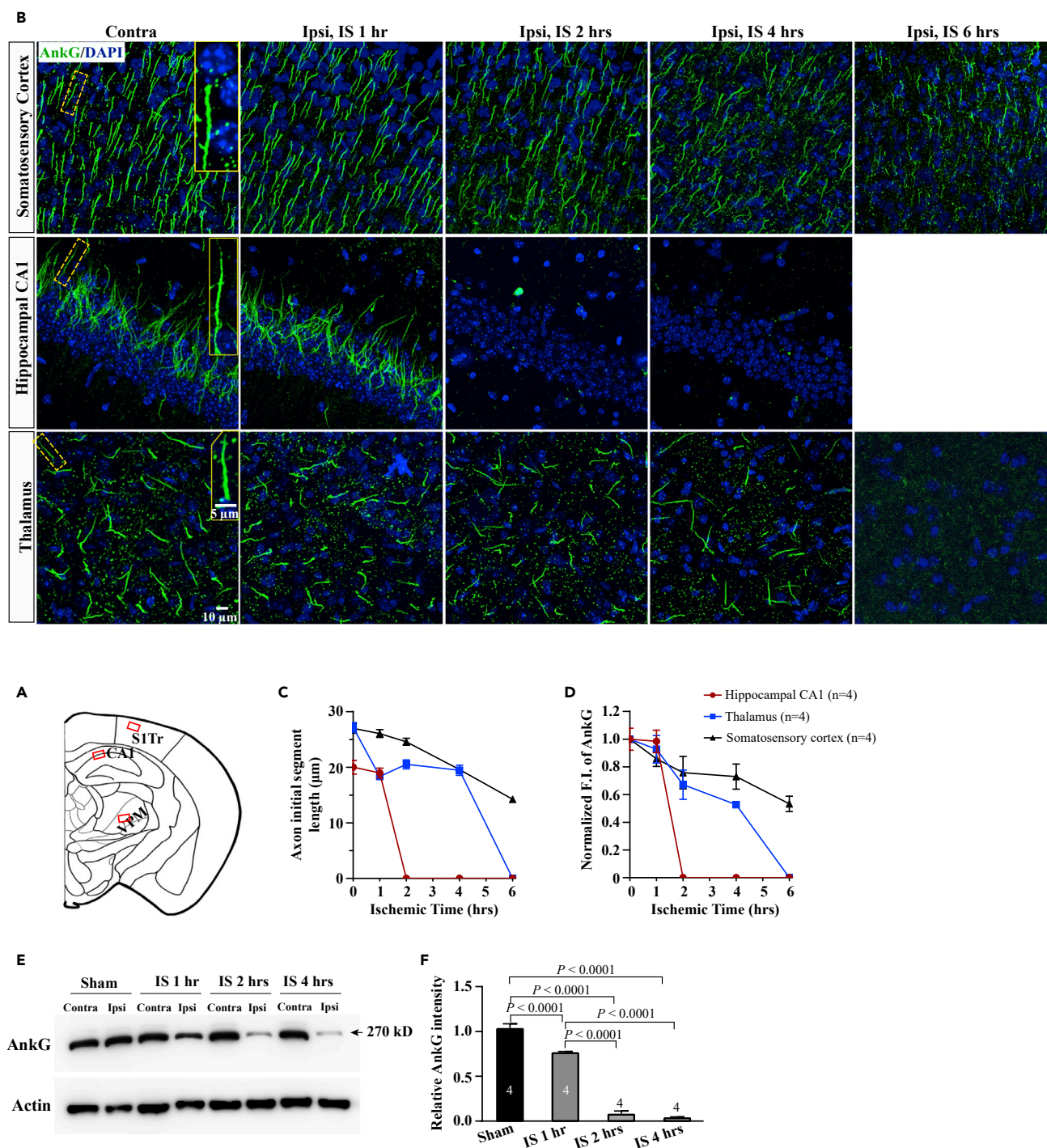
Figure 1. Ischemic Injury Causes Rapid Disruption of the AIS Cytoskeleton AnkG in the Hippocampus

(A) Schematic of the regions (boxes) studied in (B).

(B) Representative confocal images of AnkG immunostaining from the box areas (A) of the somatosensory cortex (*top*), the CA1 region (*middle*), and the thalamus (*bottom*) of mice subjected to 1 h, 2 h, 4 h, or 6 h MCAO. Insets are enlarged from the yellow box areas.

(C and D) Quantification of the length (C) and the normalized fluorescence intensity (FI) (D) of AnkG immunostaining from the somatosensory cortex (*black*), the CA1 region (*red*), and the thalamus (*blue*) after various MCAO times. The ipsilateral FI was normalized to the contralateral from the same mouse.

(E) Representative image of AnkG immunoblot of hippocampal tissue homogenates from mice subjected to various times of MCAO.

Figure 1. *Continued*
(F) Quantification of the intensity of AnkG immunoblots after various MCAO times. p values are determined using one-way ANOVA with *post hoc* Bonferroni's multiple comparisons test. N represents mouse number. Data are presented as mean ± SEM. IS, ischemic injury; Contra, contralateral; Ipsi, ipsilateral.

as the MCAO time prolonged (Figure 2E). Compared with AnkG disruption, quantitative immunoblot analyses showed ~80% retention of the full-length Na$_v$1.6 at 2-h MCAO time point and then reduced to ~70% at 4 h (Figure 2F). Together, these results suggest that Na$_v$1.6 is resistant to injury-induced decline.

AP Generation Is Impaired after Injury

Could preserved Na$_v$1.6 at the AIS generate APs in response to membrane depolarization? To address this question, we performed whole-cell electrophysiological recordings of APs on the CA1 pyramidal neurons of the contralateral and ipsilateral hippocampi following MCAO (Figure 3A). In contrast to the contralateral, we found a more positive AP threshold and a significant reduction in AP amplitude in the ipsilateral CA1 pyramidal cells after 1 h of MCAO (Figures 3B–3F), suggesting that functional alterations were prior to structural changes.

Under physiological conditions, AP propagation along the axon is required for spontaneous synaptic transmission among neurons. To examine whether impairment of AP generation could affect synaptic transmission, we performed whole-cell recordings of AP-dependent spontaneous postsynaptic currents (sPSCs) and AP-independent miniature PSCs (mPSCs) in hippocampal CA1 pyramidal neurons after injury. As we expected, sPSC frequency, but not amplitude, was significantly reduced (Figures 4A–4C), whereas neither the frequency nor the amplitude of mPSCs were altered after injury (Figures 4D–4F). These results together suggest that impairment of AP generation results in diminished synaptic transmission.

Neurofascin Is Required for Clustering Sodium Channels at the AIS after Injury

Several lines of evidence showed that Nfasc plays an important role in maintenance of sodium channel clustering at the AIS by way of association with the extracellular matrix (Hedstrom et al., 2007; Zonta et al., 2011). To test whether Na$_v$1.6 was anchored at the AIS by Nfasc after disruption of the AIS cytoskeleton, we carried out a series of experiments to demonstrate the expression of Nfasc at the AIS after injury. Nfasc remained unchanged and colocalization with Na$_v$1.6 at the AIS after 2 h of MCAO (Figures 5A and 5B). Moreover, western blotting showed no difference between the ipsilateral and contralateral hippocampi after 4 h of MCAO (Figures 5C and 5D), suggesting that Nfasc is quite resistant to injury-induced decline. These results raise a question as to whether knockdown of Nfasc would cause rapid Na$_v$1.6 disruption following MCAO.

To address this question, we took advantage of the Cre-dependent Cas9 knock-in mice to knockdown NF-186 that is predominantly expressed at the AIS. We first generated a mouse line with specific expression of Cas9 in the excitatory neurons by crossing the Cre-dependent Cas9 mouse to an Emx1-Cre driver. NF-186 sgRNA-3 that showed high efficacy of cleavage in cultured cells was selected to be constructed into the vector of adeno-associated virus (AAV)-U6-sgRNA-IRES-mCherry (Figure S4A). Next, the chimeric AAV1/2 viruses expressing sgRNA-3 were delivered via stereotactic injection into the hippocampal CA1 region of the Emx1-Cre/Cas9 mice. Seven weeks after injection, we found that the majority of NF-186 were ablated in infected neurons with sgRNA-3 AAVs (Figures S4B and S4C), which had no effect on AnkG expression at the AIS (Figure S4D). In contrast to scrambled AAVs and uninfected neurons in the same mice, Na$_v$1.6 was little detectable in the infected neurons with sgRNA-3 AAVs after 2 h of MCAO (Figures 5E–5G), suggesting that Nfasc is required for clustering Na$_v$1.6 at the AIS following ischemic injury.

Next we examined whether Nfasc anchored Na$_v$1.6 by association with the EMC after injury. Chondroitinase ABC (ChABC) that is capable of digesting the essential EMC component, the chondroitin sulfate glycosaminoglycans (CS-GAGs), was applied into the hippocampal CA1 72 h before MCAO surgery (Figures S5A–S5C). We found that ChABC treatment had no effect on the clustering of Nav1.6 and Nfasc at the AIS in the absence of MCAO (Figures S5D–S5F) but caused a rapid disruption of Na$_v$1.6 following 2 h of MCAO (Figure S5G), demonstrating that Nfasc together with the EMC clustered Na$_v$1.6.
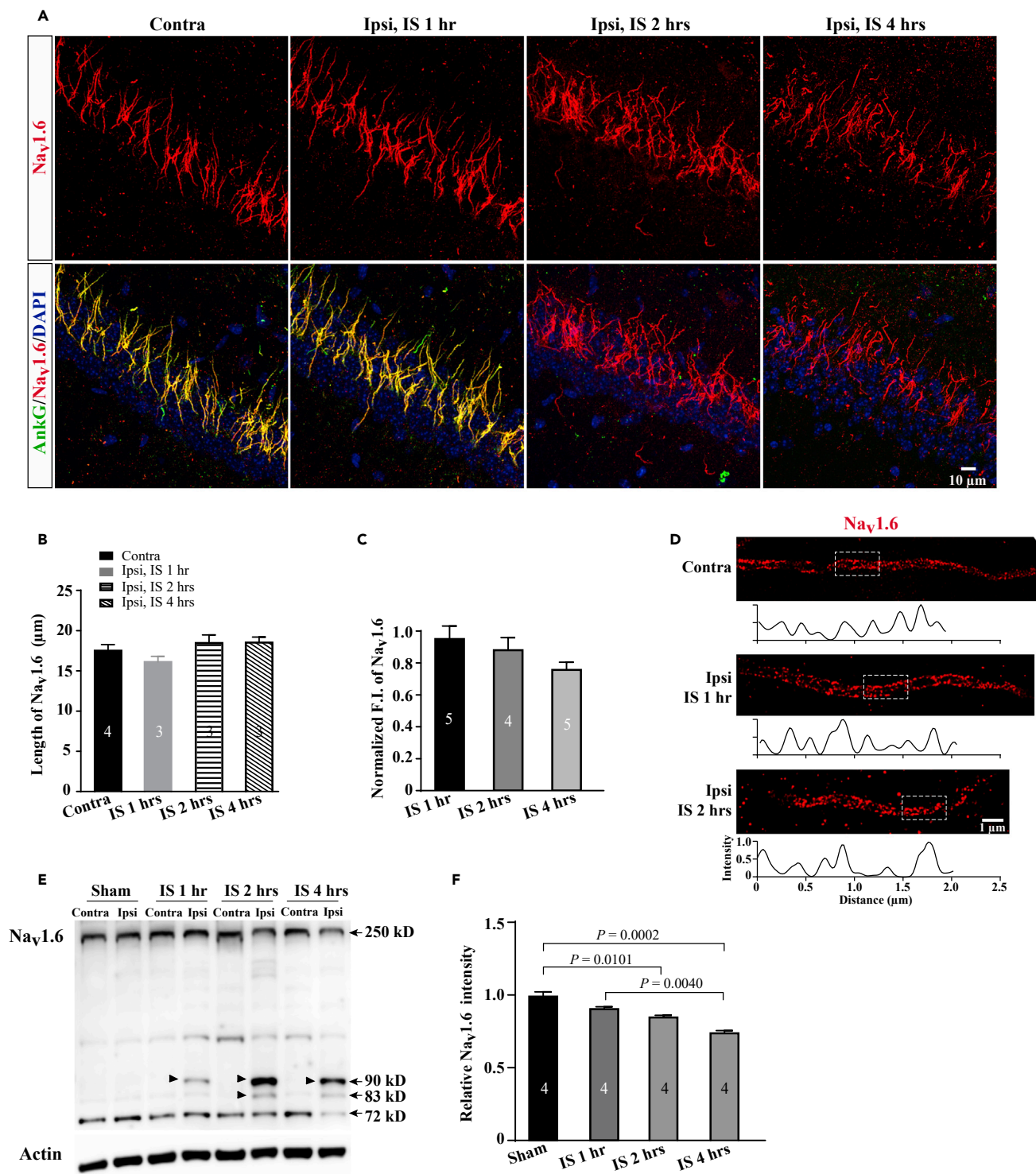
Figure 2. Na$_v$1.6 Largely Preserves at the AIS after Injury

(A) Representative confocal images of Na$_v$1.6 immunostaining in the CA1 regions from mice subjected to 1 h, 2 h, or 4 h of MCAO.

(B and C) Quantification of the length (B) and the normalized FI (C) of Na$_v$1.6 immunostaining from the CA1 pyramidal neurons after various times of MCAO.

(D) Super-resolution STED images of Na$_v$1.6 immunostaining show periodic distribution at the AIS of hippocampal CA1 pyramidal neurons after 1 h or 2 h of MCAO. Boxes indicate analyzed areas showed below.

Figure 2. *Continued*

(E) Representative image of Na$_v$1.6 immunoblot of hippocampal tissue homogenates from mice subjected to various times of MCAO. Arrow heads indicate fragments of small molecular size 110 kD and 95 kD that are proteolyzed from the full length of Na$_v$1.6.

(F) Quantification of the intensity of 250 kD Na$_v$1.6 immunoblots after various MCAO times. The ipsilateral F.I. was normalized to the contralateral from the same mouse. p values in (C) and (F) are determined using one-way ANOVA with *post hoc* Bonferroni's multiple comparisons test. N represents mouse number. Data are presented as mean ± SEM.

FK506 Fully Prevents Injury-Induced AIS Disruption

Calcineurin signaling was previously reported to play important roles in neuronal death induced by ischemic injury and in activity-dependent AIS plasticity (Evans et al., 2013; Sharkey and Butcher, 1994; Springer et al., 2000). To examine whether MCAO induced elevated calcineurin activation, which can cause NFAT to trans-locate into the nucleus, AAVs expressing fused NFAT-EGFP were injected into the hippocampus seven days prior to MCAO surgery. We found that the majority of NFAT-EGFP were located in the nucleus of the ipsi-lateral neurons compared with the cytosol of the contralateral neurons after 2 h of MCAO (Figures 6A and 6B). As disruption of the AIS cytoskeleton is an early response to injury independent of cell death, we asked whether inhibition of calcineurin with FK506 could prevent AIS disruption as well. To test this hypothesis, we
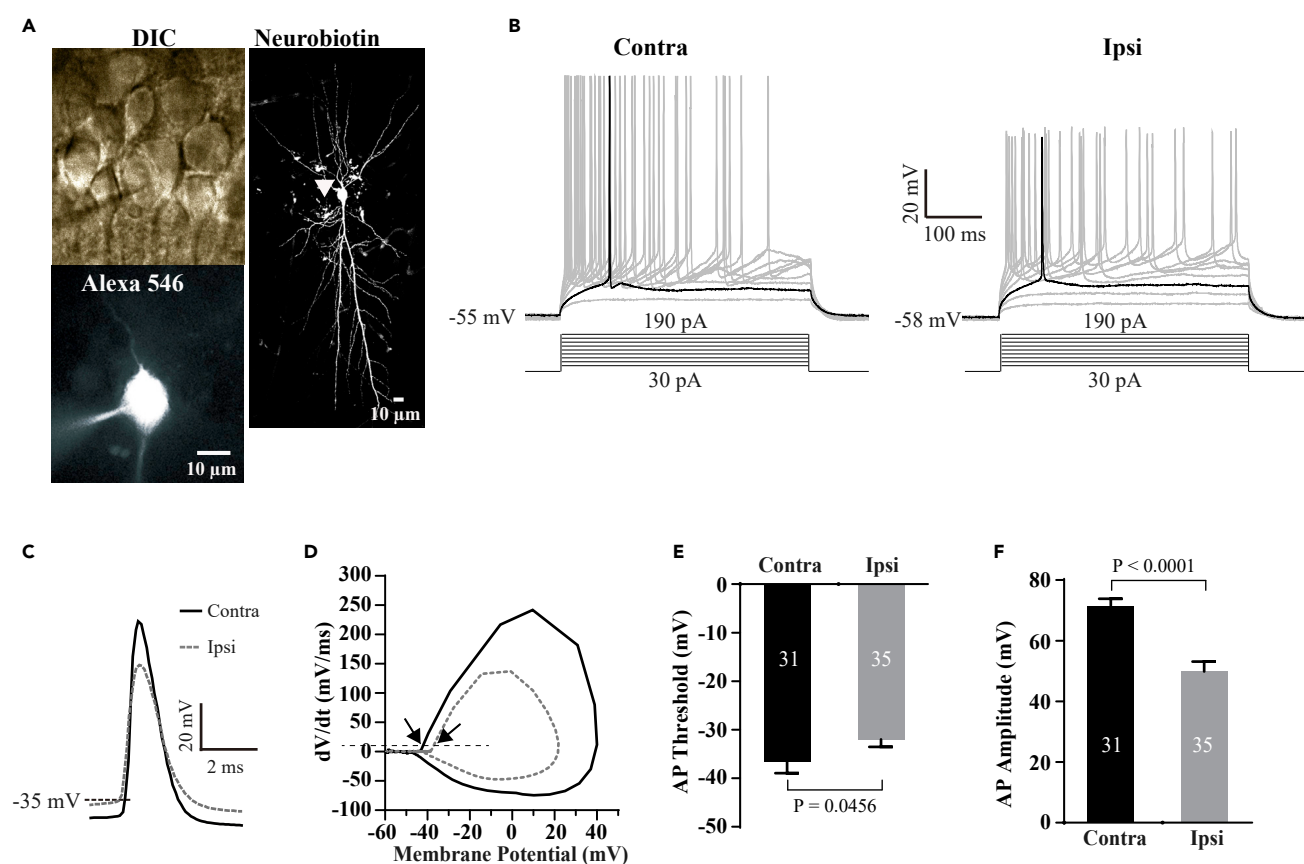
Figure 3. Ischemic Injury Impairs Action Potential Generation

(A) Representative DIC and confocal images of a recorded hippocampal CA1 pyramidal neuron filled with Alexa 546 and neurobiotin. Arrow head indicates the AIS of the recorded neuron.

(B) Sample traces of changes in membrane voltages in response to a series of step currents in 20 pA increments from +30 pA to +190 pA in CA1 pyramidal neurons from the contralateral (*left*) and ipsilateral (*right*) hippocampi following 1 h of MCAO. Highlights show the traces containing the first AP initiated in the recorded neurons.

(C) Sample traces of the first APs were overlapped from the ipsilateral and contralateral CA1 pyramidal neurons.

(D) Phase-plane plots of membrane voltage vs its change rate in response to current injection in (C). The dash line indicates the change rate of 10 mV/ms. Arrows indicate AP thresholds.

(E and F) Summary of AP threshold and amplitude in the recorded neurons from the ipsilateral and contralateral hippocampal CA1 pyramidal neurons following 1 h of MCAO. p values in (E) and (F) are determined between ipsilateral and contralateral sides using unpaired t-test. N represents neuron number recorded. Data are presented as mean ± SEM.
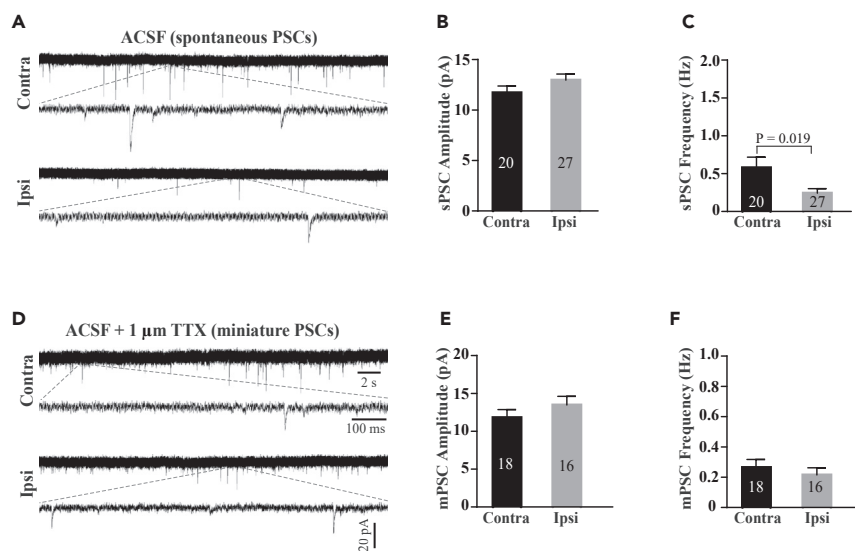
Figure 4. Ischemic Injury Impairs Action Potential-Dependent Synaptic Transmission

(A) Sample traces of spontaneous postsynaptic currents (sPSCs) recorded in the CA1 pyramidal neurons with perfusion of physiological ACSF.

(B and C) Summary of sPSC amplitude (B) and frequency (C) in the recorded CA1 pyramidal neurons from the ipsilateral and contralateral hippocampi.

(D) Sample traces of miniature postsynaptic currents (mPSCs) recorded in CA1 pyramidal neurons after perfusion of physiological ACSF containing TTX (1 μm).

(E and F) Summary of mPSC amplitude (E) and frequency (F) in the recorded CA1 pyramidal neurons from the ipsilateral and contralateral hippocampi. p value in (C) is determined between ipsilateral and contralateral sides using unpaired t-test. N represents neuron number recorded. Data are presented as mean ± SEM.

subjected mice to MCAO surgery immediately followed by intravenous injection of FK506 at two different concentrations. After 2 h of MCAO, we found little AnkG preserved at the injured AIS following treatment with 0.5 mg/kg FK506. In contrast, administration of a higher concentration of FK506 (2.5 mg/kg) completely retained AnkG at the AIS (Figures 6C and 6D). We also compared FK506 with another calcineurin inhibitor (Cyclosporin A, CsA) and a calpain inhibitor (MDL 28170) for AIS protection. Although administration of CsA (20 mg/kg) retained the majority of AnkG (Figure S6), treatment with MDL 28170 (60 mg/kg) preserved only 20% of AnkG at the injured AIS (Figure S7), consistent with a previous study showing a partial protection of calpain inhibition against AIS disruption after injury (Schafer et al., 2009). Treatment with an Hsp90 inhibitor 17-AAG (25 mg/kg) had no effect on injury-induced disruption of AnkG (Figures S8A and S8B), ruling out the possibility that FK506 and CsA acted through inhibiting the Hsp90 stress response pathway (Owens-Grillo et al., 1995). Moreover, injury-induced NFAT-EGFP nuclear translocation was blocked by FK506 and CsA (Figures 6A and 6B). These results together suggest that inhibition of calcineurin with FK506 is sufficient to fully protect the AIS cytoskeleton from ischemic injury.

Next we further examined the function of preserved AIS cytoskeleton by FK506 using whole-cell electrophysiological recordings of hippocampal CA1 pyramidal cells. We found no significant difference in AP amplitude and threshold between the ipsilateral and contralateral hippocampi of FK506-treated MCAO mice (Figures 6E–6H). Likewise, sPSC frequency was no longer changed following MCAO in FK506-treated mice (Figures 6I–6K).

To address whether protection at the cellular level led to recovery of cognitive function, we subjected the MCAO-, sham-, and FK506-treatment mice to the hidden-platform version of Morris watermaze task with spatial cues (Morris et al., 1982) and new object recognition tasks for examining spatial and non-spatial memory, respectively. We chose the paradigm of 30-min transient MCAO (tMCAO) followed by re-perfusion because this mimicked 2 h of MCAO showing AnkG disruption but Na$_v$1.6 and Nfasc preservation at the AIS (Figures 7A, S9A, and S9B). During the consecutive five-day training, the latencies for revealing the hidden platform were gradually decreased for both sham and MCAO mice, whereas the sham group achieved a significant shorter latency from the training day 2 compared with the MCAO mice
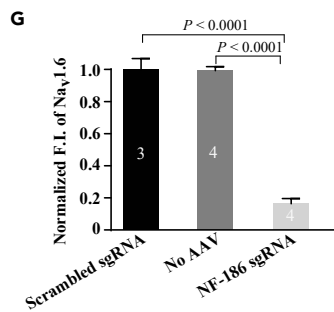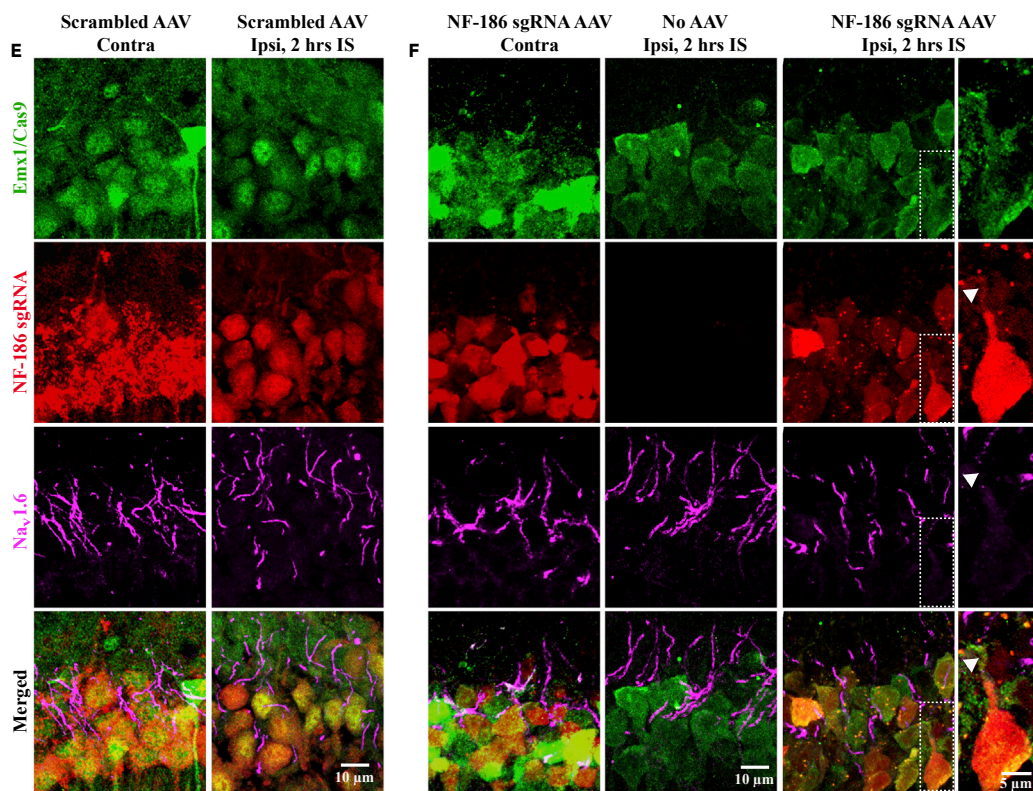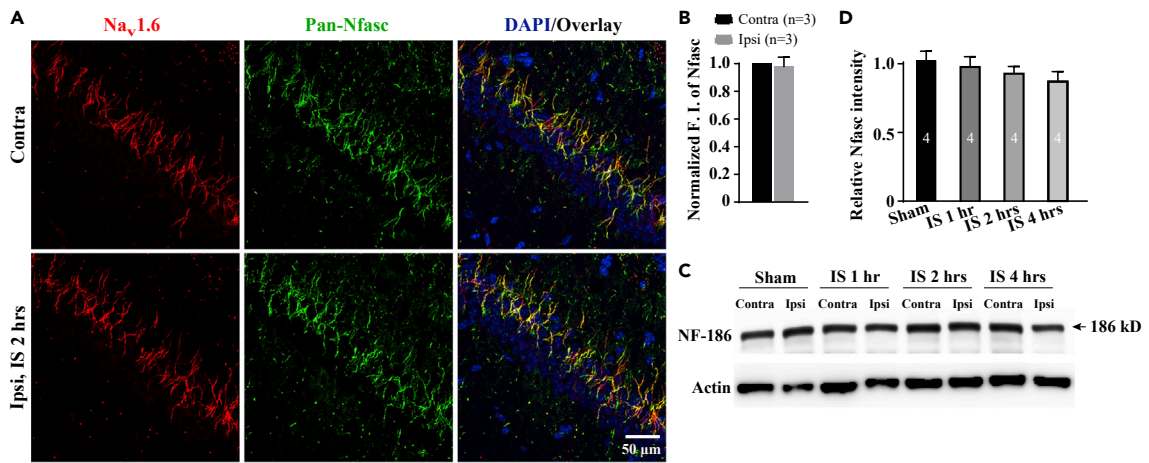
Figure 5. Nfasc Is Required for Na$_v$1.6 Clustering at the AIS after Ischemic Injury

(A) Representative confocal images of Nfasc (*green*) and Na$_v$1.6 (*red*) immunostaining in the hippocampal CA1 regions of mice subjected to 2 h of MCAO.

(B) Quantification of the normalized F.I. of Nfasc immunostaining in (A).

(C and D) Representative images (C) and quantification (D) of NF-186 immunoblot of hippocampal homogenates from mice subjected to sham or various times of MCAO.

(E–G) Representative confocal images (E and F) and quantification (G) of the normalized F.I. of Na$_v$1.6 (*magenta*) immunostaining in the presence or absence of NF-186 in hippocampal pyramidal neurons after 2 h of MCAO. Scrambled or NF-186 sgRNA AAVs were delivered into the hippocampus of Emx1-Cre-dependent Cas9 expressing mice seven weeks before MCAO surgery. The scrambled sgRNA serves as a control. The ipsilateral F.I. was normalized to the contralateral from the same mouse. Note that Na$_v$1.6 staining is not present at the AIS (Arrow heads) of a neuron expressing Cas9 (*green*) and NF-186 sgRNA (*red*). Boxes are enlarged in the right panels. p values in (F) are determined using one-way ANOVA with *post hoc* Bonferroni's multiple comparisons test. N indicates the number of mice. Data are presented as mean $\pm$ SEM.

(Figure 7B). For the probing task conducted on day 6, the sham group spent significantly more time in the target quadrant than the MCAO group who displayed no preference for the four quadrants (Figure 7C), and the sham group had more platform crossings than the MCAO group (Figures 7D and S9C), suggesting that the hippocampal-dependent spatial learning and memory is impaired after ischemic injury. These differences between the sham and MCAO groups were not due to changes in the swimming speed (Figures S9D and S9E). Mostly importantly, we found time spent in the target quadrant and platform crossings for FK506-treated MCAO mice similar to that of the sham group in the Morris watermaze task (Figures 7C, 7D, and S9C), indicating that spatial learning and memory of MCAO mice is fully protected by FK506.

Next, we subjected mice to new object recognition task for testing non-spatial memory. Generally, the new object recognition task mostly represents functions of the perirhinal and prefrontal cortex (Albasser et al., 2015; Barker and Warburton, 2011; Winters et al., 2004), although it is yet under debate (Cohen et al., 2013). After a short-term recognition for getting familiar with two objects, the sham-, MCAO-, and FK506-treatment groups showed no difference for the time spent on the new or familiar objects (Figure 7E). Three groups preferred to explore the novel object compared with the familiar one (Figure 7F), suggesting that non-spatial memory is not impaired after ischemic injury.

Taken together, these results suggest that inhibition of calcineurin with FK506 fully protect not only the cytoskeletal structure but also AIS function and spatial learning and memory following ischemic injury.

DISCUSSION

The AIS cytoskeleton rapidly and irreversibly disassembles in response to injury. Given that the AIS plays a pivotal role in synaptic transmission by generating APs, disruption of the AIS cytoskeleton could lead to many neurological disorders associated with damaged brain regions. By comparing the peri-infarct regions, we found that the AIS cytoskeleton was more rapidly disrupted in the hippocampus than the striatum and somatosensory cortex, consistent with previous findings demonstrating that neuronal degeneration selectively occurred in the hippocampus and that hippocampal-dependent spatial memory tended to be impaired after injury in animal models and human patients (Bartsch et al., 2015; Pulsinelli et al., 1982; Schmidt-Kastner and Freund, 1991).

Na$_v$ Channels Are Resistant to Injury-Induced Decline at the AIS

AnkG is crucial for AIS assembly during development, and either genetic ablation or silence of AnkG expression by shRNA failed to recruit Na$_v$ channels, NF-186, NrCAM, and βIV-spectrin into the AIS (Hedstrom et al., 2007; Huang and Rasband, 2018; Jenkins and Bennett, 2001; Zhou et al., 1998). A previous study reported that Na$_v$1.6 and AnkG were concurrently disrupted in the infarct core area of the cortex in a focal ischemia/reperfusion (I/R, 90 min of MCAO followed by reperfusion) (Schafer et al., 2009). To examine the stability of Na$_v$, we prolonged MCAO up to 6 h and examined an alteration in Na$_v$1.6 density in the peri-infarct hippocampus. In contrast to complete AnkG disruption after 2 h of MCAO, we found that the majority of Na$_v$1.6 preserved at the AIS till 6 h of MCAO.

Na$_v$1.6 is mainly distributed in the distal AIS and responsible for AP generation due to its activation at a low threshold (Hu et al., 2009). AP generation is impaired in the CA1 pyramidal neurons, whereas Na$_v$1.6 density is not altered at the time point of 1 h of MCAO. Because breakdown fragments of Na$_v$1.6 were observed at this time point, a small amount of Na$_v$1.6 proteolysis might be enough to impair AIS function but did not influence the intensity. But we cannot rule out other possibilities that (1) the density of other Na$_v$ channels such as Na$_v$1.2 that is predominantly located in the proximal AIS was reduced
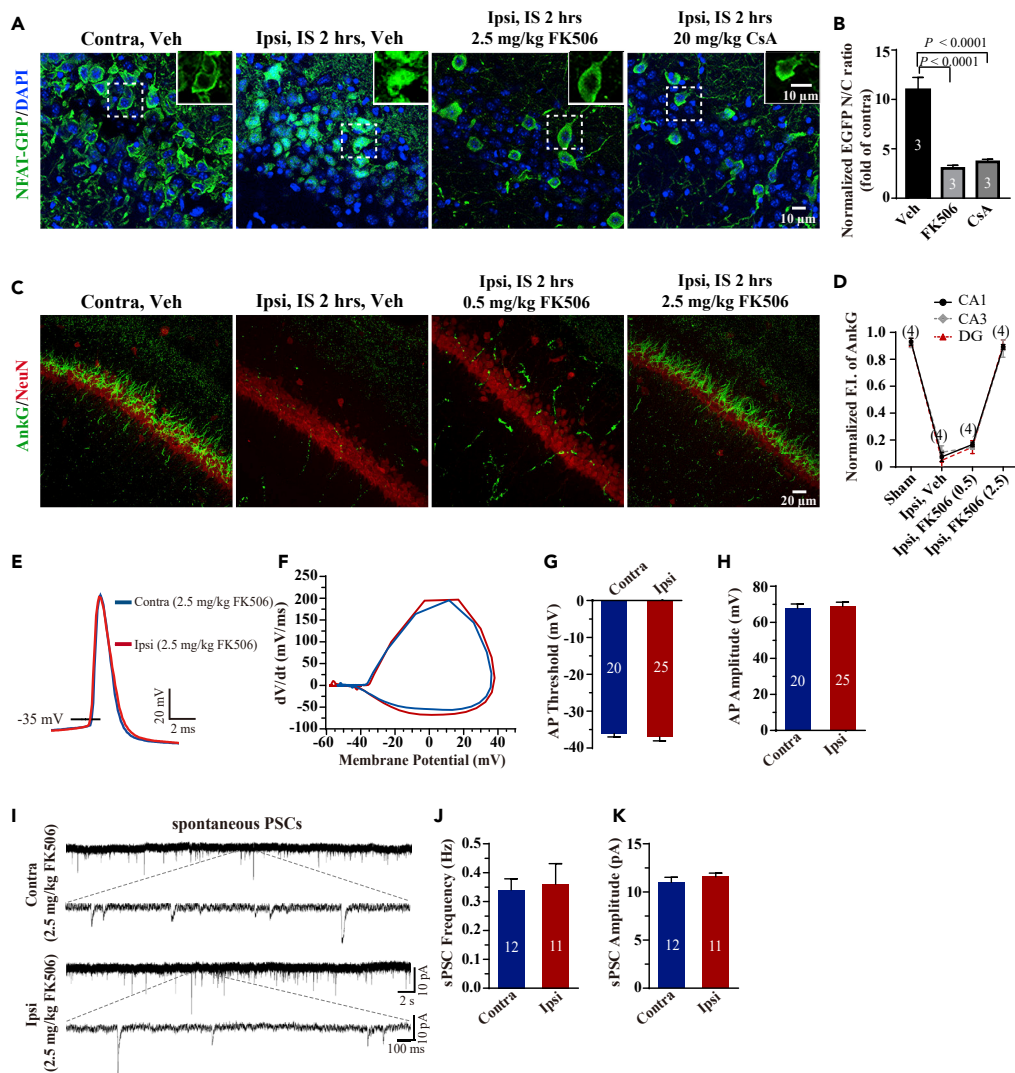
Figure 6. FK506 Completely Protects the AIS Cytoskeleton and Function after Injury

(A and B) Representative confocal images (A) and quantification (B) show translocation of NFAT-GFP into the nucleus following injury; but this is blocked by 2.5 mg/kg FK506 or 20 mg/kg CsA. Insets are enlarged from the boxes. The ipsilateral F.I. ratio of the nuclear NFAT-EGFP to the cytosol is normalized to that of the contralateral from the same mouse.

(C) Representative confocal images of AnkG immunostaining of the CA1 regions from MCAO mice treated with vehicle (Veh), 0.5 mg/kg FK506 or 2.5 mg/kg FK506.

(D) Quantification of AnkG intensity normalized to the corresponding contralateral for different treatments.

(E–H) The overlap of sample traces (E), phase-plane plots (F), and summary of the threshold (G) and amplitude (H) of the first APs recorded from the ipsilateral and contralateral hippocampal CA1 pyramidal neurons of 2.5 mg/kg FK506 treatment.

(I–K) Sample traces (I) and summary of sPSC amplitude (J) and frequency (K) recorded from CA1 pyramidal neurons of 2.5 mg/kg FK506 treatment. p values in (B) are determined using one-way ANOVA with *post hoc* Bonferroni's multiple comparisons test. N in (B and D) denotes the number of mice and N in (F and G) indicates neuron number recorded. Data are presented as mean $\pm$ SEM.

after injury; and (2) Na_v phosphorylation was increased after injury. In support of this, p38-mitogen-activated protein kinases (MAPKs) has been reported to be activated in the brain following ischemic injury (Alessandrini et al., 1999; Barone et al., 2001; Sugino et al., 2000), and p38 activation then phosphorylates $Na_v1.6$ serine 553, which can result in a reduction of $Na_v1.6$ current density (Wittmack et al., 2005).

Given that the majority of $Na_v1.6$ preserved in the hippocampal AIS after disruption of the cytoskeleton in response to injury, we examined the hippocampal-dependent spatial learning and memory and the
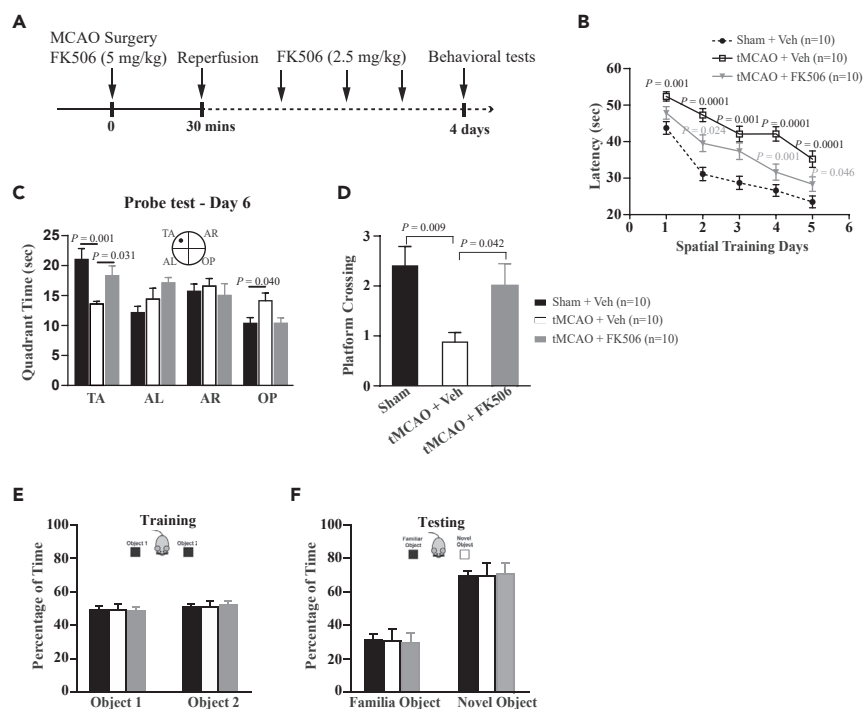
Figure 7. FK506 Fully Protects Hippocampal-Dependent Spatial Learning and Memory after Injury

(A) Schematic of the experimental paradigm of mice subjected to transient MCAO (tMCAO, 30 min of MCAO followed by reperfusion of four days) for behavioral tests.

(B–D) Behavioral test of standard hidden platform watermaze tasks for three groups of mice: sham + Veh, tMCAO + Veh, and tMCAO + FK506 (2.5 mg/kg). (B) Quantification of the latency to reach the platform for three groups of mice during the training days. The latency for the group of tMCAO + Veh is significant longer than those of the two groups of sham + Veh and tMCAO + FK506, but there are only significant differences in latency between sham + Veh and tMCAO + FK506 at day 2 (p = 0.007) and day 3 (p = 0.009). (C and D) Quantification of time spent in the quadrant areas of the maze (C) and the number of platform crossings (D) for three groups of mice in the probing test day (day 6). Time spent in TA and the number of platform crossings for the group of tMCAO + Veh are significantly reduced than those of the two groups of sham + Veh and tMCAO + FK506, but there is no difference between sham + Veh and tMCAO + FK506.

(E and F) Quantification of time spent on two identical objects during training (E) and on the familiar object and novel object during test (F) for three groups. Time spent on the novel object is significantly longer than that of the familiar object, but there is no difference in time spent on the novel object between three groups. TA, target quadrant; AL, adjacent left quadrant; AR, adjacent right quadrant, and OP, opposite quadrant. p values in (B and C) and in (D) are determined using two-way and one-way ANOVA with *post hoc* Bonferroni's multiple comparisons test, respectively. p values (gray) indicate significance between tMCAO + FK506 and tMCAO + Veh. p values (black) indicate significance between tMCAO + Veh and sham + Veh. N denotes the number of mice studied. Data are presented as means ± SEM.

perirhinal cortex-involved non-spatial memory in a mouse model of I/R injury (30 min of MCAO followed by reperfusion), which have mostly mimicked the condition of 2 h of MCAO in terms of AnkG disruption and retentions of $Na_v1.6$ and Nfasc. We found that ischemic injury caused severe impairment of spatial memory rather than non-spatial memory, implicating that the hippocampus is more likely damaged than the perirhinal cortex.

Nfasc Is Required for Na_vChannel Maintenance at the AIS after Injury

Unlike AnkG, Nfasc is not required for AIS assembly but might stabilize the AIS ion channels by interacting with both AnkG and brevican-based ECM (Hedstrom et al., 2007). Consistent with this idea, our results demonstrate that Nfasc and the vast majority of $Na_v1.6$ preserve at the AIS in the absence of AnkG following a prolonged ischemic injury. Knockout of Nfasc in Cre-dependent cas9 knock-in mice and destruction of the chondroitin sulfate proteoglycans (CSPGs) with ChABC abolish $Na_v1.6$ clustering at the AIS after injury, suggesting that Nfasc contributes to maintenance of $Na_v1.6$ after injury. Because the current model of the AIS architecture shows that Nfasc does not directly interact with the pore-forming α subunits of $Na_v1.6$ at the AIS domain, how Nfasc stabilizes $Na_v1.6$ in the absence of AnkG after injury needs further investigations.

Previous studies have reported that a regulatory subunit $Na_v\beta1$ directly interacts with NF-186 and NrCAM (McEwen and Isom, 2004), and Navβ4 associates with $Na_v\alpha$ via a covalent disulfide at the AIS (Buffington and Rasband, 2013). Therefore, we speculate that the β subunit may serve as a linker between Nfasc and $Na_v1.6$ α subunits although other possibilities cannot be ruled out. For instance, some unidentified anchoring molecules that directly interact with both Nfasc and $Na_v\alpha$ can cluster $Na_v1.6$ at the AIS. Or under pathophysiological conditions Nfasc directly binds to the $Na_v1.6$ α subunits in the absence of AnkG. At least, a previous study showed that an Nfasc-binding protein brevican was upregulated in the optic nerve following ischemia (Reinhard et al., 2017). Further experiments are needed to address these questions.

Potential Mechanisms Underlying AIS Protection by FK506 after Injury

Given that the majority of $Na_v1.6$ preserved in the hippocampal AIS after disruption of the cytoskeleton in response to injury, we examined the hippocampal-dependent spatial learning and memory and the perirhinal cortex-involved non-spatial memory in a mouse model of I/R injury (30 min of MCAO followed by reperfusion), which have mostly mimicked the condition of 2 h of MCAO in terms of AnkG disruption and retentions of $Na_v1.6$ and Nfasc. We found that ischemic injury caused severe impairment of spatial memory rather than non-spatial memory, implicating that the hippocampus is more likely damaged than the perirhinal cortex. Treatment with a calcineurin inhibitor FK506 completely prevented injury-induced disruption of the AIS cytoskeleton, AIS function, and spatial memory impairments. Calpain has been previously reported to partially proteolyze the AIS cytoskeletal proteins following ischemic injury, raising the possibility that in addition to calpain other proteases are involved in the breakdown of the cytoskeleton protein. How calcineurin works in concert with calpain or other proteases remains an open question.

How does injury cause a cytosolic Ca^{2+} surge to activate calcineurin? Blockade of NMDA receptors is previously reported to have no effect on disruption of the AIS cytoskeleton after injury. In this study, we found that blockade of L-type voltage-gated calcium channels (VGCCs) prevents disruption of the AIS cytoskeleton after injury (Figure S8C), suggesting that Ca^{2+} influx through VGCCs activated calcineurin to trigger injury-dependent AIS disruption. This is consistent with previous studies demonstrating that blockade of the L-type VGCC prevents calcineurin-mediated activity-dependent AIS plasticity and activation of the caspase apoptotic cascade (Evans et al., 2013; Springer et al., 2000). However, inhibition of purinergic P2X7 receptors had no effect on AIS disruption induced by 2 h of MCAO (Figure S8C), which is inconsistent with a previous report showing that inhibition of P2X7 receptors could prevent AIS disruption in a rat model of ischemia/reperfusion (I/R, 90 min of MCAO followed by reperfusion) (Del Puerto et al., 2015). This discrepancy may be due to different animal species, ischemic time, and/or injury models as well as different treatment types. In contrast to our study that drugs were applied immediately following surgery, P2X7 receptor inhibitors were administered 3 h after injury in the previous study.

In conclusion, we have shown that calcineurin signaling regulates disruption of the AIS cytoskeletal protein after injury. Owing to protection of cell survival and AIS integrity, calcineurin inhibitors might be potential therapeutic drugs for treating ischemic patients.

Limitations of the Study

One caveat of this study is that sPSCs recorded from CA1 pyramidal cells demonstrate AIS function of the presynaptic neurons rather than postsynaptic CA1 pyramidal cells. Moreover, given that genetic knockout of calcineurin in the forebrain has been shown to impair synaptic plasticity and working memory associated with the hippocampus (Zeng et al., 2001), maintaining certain level of calcineurin activity is crucial for normal brain function. Thus future work focuses on whether partial and transient inhibition of calcineurin would be better suited to be a therapeutic treatment and for determining the optimal window for calcineurin inhibitors applied into ischemia patients.

METHODS

All methods can be found in the accompanying Transparent Methods supplemental file.

SUPPLEMENTAL INFORMATION

Supplemental Information can be found online at https://doi.org/10.1016/j.isci.2020.100880.

iScience

CellPress

AUTHOR CONTRIBUTIONS

Y. Z., X. W., Z. G., and S. H. conceived the project and designed the experiments. Y. Z. generated data for immunostaining, immunoblot, and animal behavioral tests. X. W. did electrophysiological recordings, behavioral tests, and immunostaining experiments. X. C. made AAV viruses. J. L. designed sgRNAs. C. T. performed super-resolution imaging. J. C. collected a part of confocal images. C. X. performed behavioral experiments. Y. Z., X. W., G. X., and S. H. wrote the paper. All of the authors discussed the results and contributed to the preparation of the manuscript.

DECLARATION OF INTERESTS

The authors declare no competing financial interests.

REFERENCES

Albasser, M.M., Olarte-Sanchez, C.M., Amin, E., Brown, M.W., Kinnavane, L., and Aggleton, J.P. (2015). Perirhinal cortex lesions in rats: novelty detection and sensitivity to interference. Behav.Neurosci. *129*, 227–243.

Alessandrini, A., Namura, S., Moskowitz, M.A., and Bonventre, J.V. (1999). MEK1 protein kinase inhibition protects against damage resulting from focal cerebral ischemia. Proc. Natl. Acad. Sci. U S A *96*, 12866–12869.

Barker, G.R., and Warburton, E.C. (2011). When is the hippocampus involved in recognition memory? J. Neurosci. *31*, 10721–10731.

Barone, F.C., Irving, E.A., Ray, A.M., Lee, J.C., Kassis, S., Kumar, S., Badger, A.M., Legos, J.J., Erhardt, J.A., Ohlstein, E.H., et al. (2001). Inhibition of p38 mitogen-activated protein kinase provides neuroprotection in cerebral focal ischemia. Med. Res. Rev. *21*, 129–145.

Bartsch, T., Dohring, J., Reuter, S., Finke, C., Rohr, A., Brauer, H., Deuschl, G., and Jansen, O. (2015). Selective neuronal vulnerability of human hippocampal CA1 neurons: lesion evolution, temporal course, and pattern of hippocampal damage in diffusion-weighted MR imaging. J. Cereb. Blood Flow Metab. *35*, 1836–1845.

Buffington, S.A., and Rasband, M.N. (2013). Na+ channel-dependent recruitment of Navbeta4 to axon initial segments and nodes of Ranvier. J. Neurosci. *33*, 6191–6202.

Cohen, S.J., Munchow, A.H., Rios, L.M., Zhang, G., Asgeirsdottir, H.N., and Stackman, R.W., Jr. (2013). The rodent hippocampus is essential for nonspatial object memory. Curr. Biol. *23*, 1685–1690.

Czogalla, A., and Sikorski, A.F. (2005). Spectrin and calpain: a 'target' and a 'sniper' in the pathology of neuronal cells, [Review]. Cell. Mol. Life Sci. *62*, 1913–1924.

Del Puerto, A., Fronzaroli-Molinieres, L., Perez-Alvarez, M.J., Giraud, P., Carlier, E., Wandosell, F., Debanne, D., and Garrido, J.J. (2015). ATP-P2X7 receptor modulates axon initial segment composition and function in physiological conditions and brain injury. Cereb.Cortex *25*, 2282–2294.

Evans, M.D., Sammons, R.P., Lebron, S., Dumitrescu, A.S., Watkins, T.B., Uebele, V.N., Renger, J.J., and Grubb, M.S. (2013). Calcineurin signaling mediates activity-dependent relocation of the axon initial segment. J. Neurosci. *33*, 6950–6963.

Hedstrom, K.L., Xu, X., Ogawa, Y., Frischknecht, R., Seidenbecher, C.I., Shrager, P., and Rasband, M.N. (2007). Neurofascin assembles a specialized extracellular matrix at the axon initial segment. J.Cell Biol. *178*, 875–886.

Hinman, J.D., Rasband, M.N., and Carmichael, S.T. (2013). Remodeling of the axon initial segment after focal cortical and white matter stroke. Stroke *44*, 182–189.

Hu, W., Tian, C., Li, T., Yang, M., Hou, H., and Shu, Y. (2009). Distinct contributions of Na(v)1.6 and Na(v)1.2 in action potential initiation and backpropagation. Nat. Neurosci. *12*, 996–1002.

Huang, C.Y., and Rasband, M.N. (2018). Axon initial segments: structure, function, and disease, [Review]. Ann. N. Y. Acad. Sci. *1420*, 46–61.

Jenkins, S.M., and Bennett, V. (2001). Ankyrin-G coordinates assembly of the spectrin-based membrane skeleton, voltage-gated sodium channels, and L1 CAMs at Purkinje neuron initial segments. J.Cell Biol. *155*, 739–746.

Kole, M.H., Ilschner, S.U., Kampa, B.M., Williams, S.R., Ruben, P.C., and Stuart, G.J. (2008). Action potential generation requires a high sodium channel density in the axon initial segment. Nat. Neurosci. *11*, 178–186.

McEwen, D.P., and Isom, L.L. (2004). Heterophilic interactions of sodium channel beta1 subunits with axonal and glial cell adhesion molecules. J. Biol. Chem. *279*, 52744–52752.

Morris, R.G., Garrud, P., Rawlins, J.N., and O'Keefe, J. (1982). Place navigation impaired in rats with hippocampal lesions. Nature *297*, 681–683.

Nudo, R.J. (2013). Recovery after brain injury: mechanisms and principles. Front. Hum.Neurosci. *7*, 887.

Owens-Grillo, J.K., Hoffmann, K., Hutchison, K.A., Yem, A.W., Deibel, M.R., Jr., Handschumacher, R.E., and Pratt, W.B. (1995). The cyclosporin A-binding immunophilin CyP-40 and the FK506-binding immunophilin hsp56 bind to a common site on hsp90 and exist in independent cytosolic heterocomplexes with the untransformed glucocorticoid receptor. J. Biol. Chem. *270*, 20479–20484.

Popp, A., Jaenisch, N., Witte, O.W., and Frahm, C. (2009). Identification of ischemic regions in a rat model of stroke. PLoS One 4, e4764.

Pulsinelli, W.A., Brierley, J.B., and Plum, F. (1982). Temporal profile of neuronal damage in a model of transient forebrain ischemia. Ann. Neurol. 11, 491–498.

Ratcliffe, N.R., Kennedy, S.M., and Morganelli, P.M. (2001). Immunocytochemical detection of Fcgamma receptors in human atherosclerotic lesions. Immunol.Lett. 77, 169–174.

Reinhard, J., Renner, M., Wiemann, S., Shakoor, D.A., Stute, G., Dick, H.B., Faissner, A., and Joachim, S.C. (2017). Ischemic injury leads to extracellular matrix alterations in retina and optic nerve. Sci. Rep. 7, 43470.

Schafer, D.P., Jha, S., Liu, F., Akella, T., McCullough, L.D., and Rasband, M.N. (2009). Disruption of the axon initial segment cytoskeleton is a new mechanism for neuronal injury. J. Neurosci. 29, 13242–13254.

Schmidt-Kastner, R., and Freund, T.F. (1991). Selective vulnerability of the hippocampus in brain ischemia. Neuroscience 40, 599–636.

Sharkey, J., and Butcher, S.P. (1994). Immunophilins mediate the neuroprotective effects of FK506 in focal cerebral ischaemia. Nature 371, 336–339.

Springer, J.E., Azbill, R.D., Nottingham, S.A., and Kennedy, S.E. (2000). Calcineurin-mediated BAD dephosphorylation activates the caspase-3 apoptotic cascade in traumatic spinal cord injury. J. Neurosci. 20, 7246–7251.

Sugino, T., Nozaki, K., Takagi, Y., Hattori, I., Hashimoto, N., Moriguchi, T., and Nishida, E. (2000). Activation of mitogen-activated protein kinases after transient forebrain ischemia in gerbil hippocampus. J. Neurosci. 20, 4506–4514.

White, B.C., Sullivan, J.M., DeGracia, D.J., O'Neil, B.J., Neumar, R.W., Grossman, L.I., Rafols, J.A., and Krause, G.S. (2000). Brain ischemia and reperfusion: molecular mechanisms of neuronal injury, [Review]. J. Neurol. Sci. 179, 1–33.

Wieloch, T., and Nikolich, K. (2006). Mechanisms of neural plasticity following brain injury, [Review]. Curr.Opin.Neurobiol. 16, 258–264.

Winters, B.D., Forwood, S.E., Cowell, R.A., Saksida, L.M., and Bussey, T.J. (2004). Double dissociation between the effects of peri-postrhinal cortex and hippocampal lesions on tests of object recognition and spatial memory: heterogeneity of function within the temporal lobe. J. Neurosci. 24, 5901–5908.

Wittmack, E.K., Rush, A.M., Hudmon, A., Waxman, S.G., and Dib-Hajj, S.D. (2005). Voltage-gated sodium channel Nav1.6 is modulated by p38 mitogen-activated protein kinase. J. Neurosci. 25, 6621–6630.

Zeng, H., Chattarji, S., Barbarosie, M., Rondi-Reig, L., Philpot, B.D., Miyakawa, T., Bear, M.F., and Tonegawa, S. (2001). Forebrain-specific calcineurin knockout selectively impairs bidirectional synaptic plasticity and working/episodic-like memory. Cell 107, 617–629.

Zhou, D., Lambert, S., Malen, P.L., Carpenter, S., Boland, L.M., and Bennett, V. (1998). AnkyrinG is required for clustering of voltage-gated Na channels at axon initial segments and for normal action potential firing. J.Cell Biol. 143, 1295–1304.

Zonta, B., Desmazieres, A., Rinaldi, A., Tait, S., Sherman, D.L., Nolan, M.F., and Brophy, P.J. (2011). A critical role for Neurofascin in regulating action potential initiation through maintenance of the axon initial segment. Neuron 69, 945–956.
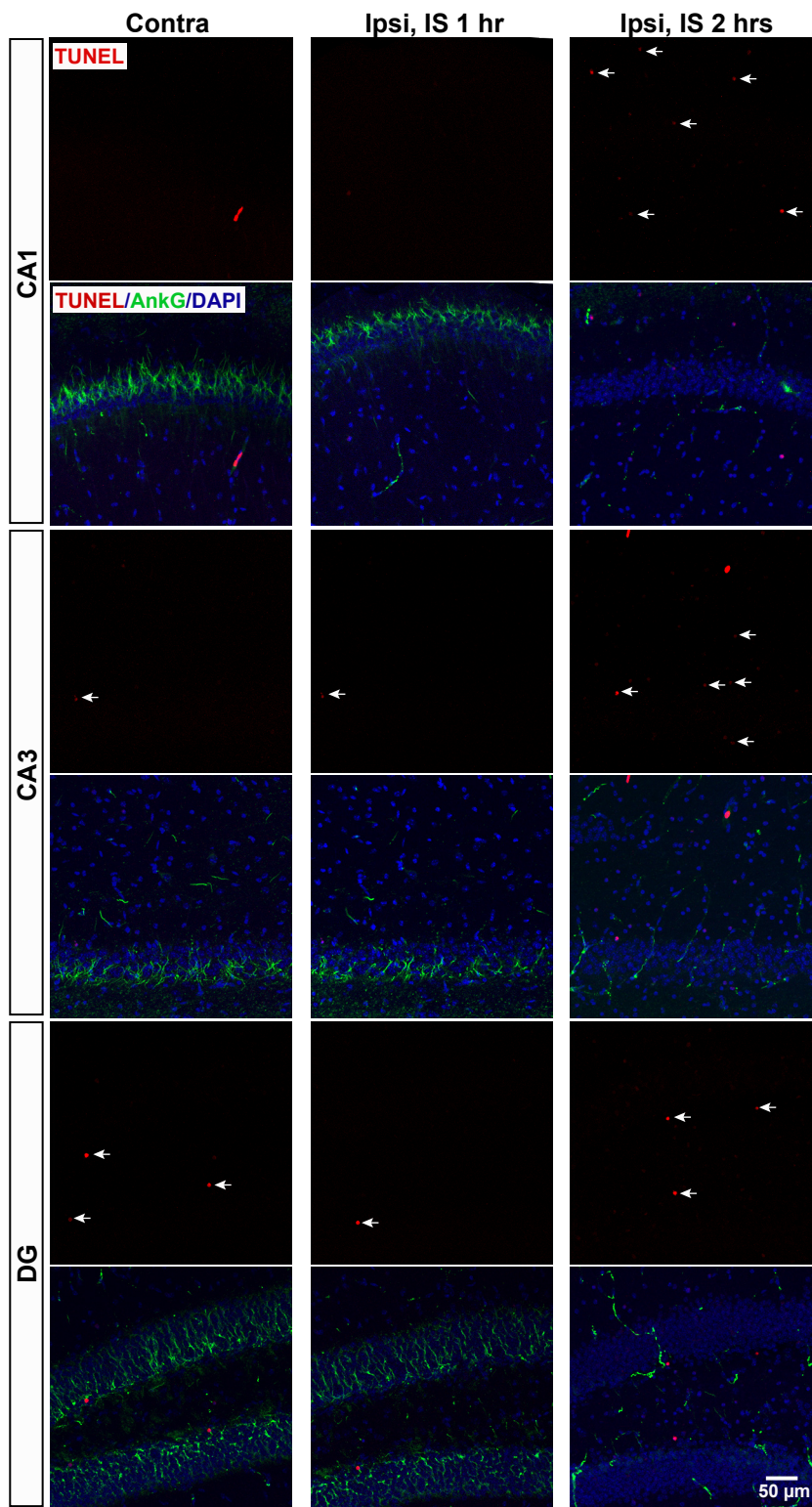
Supplemental Information

Calcineurin Signaling Mediates

# Disruption of the Axon Initial

Segment Cytoskeleton after Injury

Yanan Zhao, Xuanyuan Wu, Xin Chen, Jianan Li, Cuiping Tian, Jiangrui Chen, Cheng Xiao, Guisheng Zhong, and Shuijin He

Supplemental Figures

Figure S1. Cell death is slightly increased in the hippocampus after 2 hrs MCAO, related to Figure 1. Representative confocal images of TUNEL (*red*) and AnkG immunostaining (*green*) in the hippocampal CA1, CA3 and DG regions of mice subjected to 1 hr or 2 hrs of MCAO. A slight increase in the number of TUNEL-positive cells is only observed in the ipsilateral hippocampus after 2 hrs of MCAO. Arrows indicate TUNEL-positive cells. Note that AnkG is completely disrupted in the CA3 and DG regions after 2 hrs MCAO.

A

B

C

D
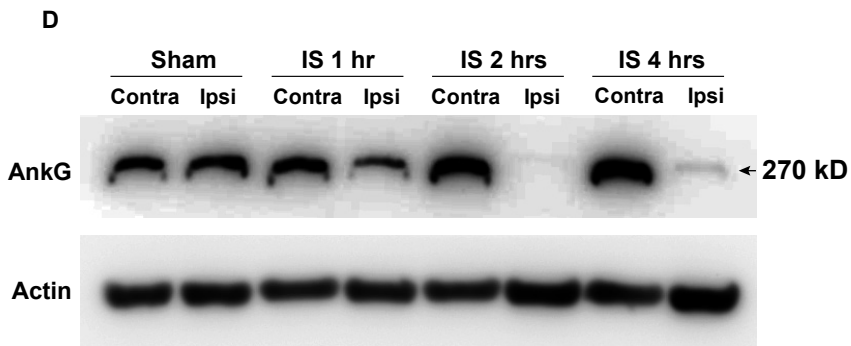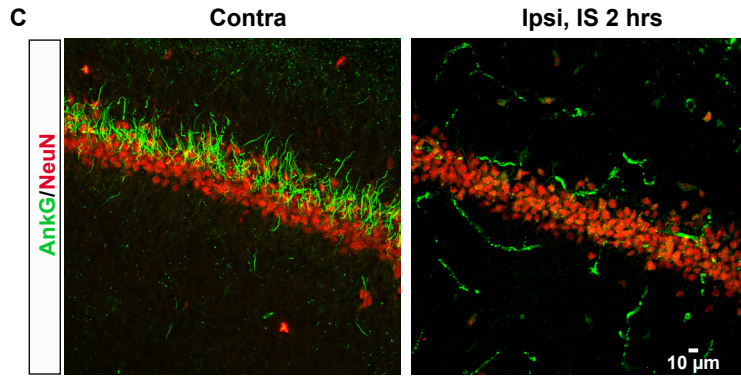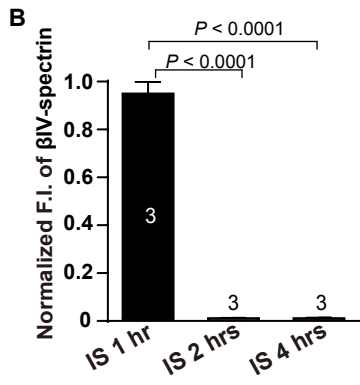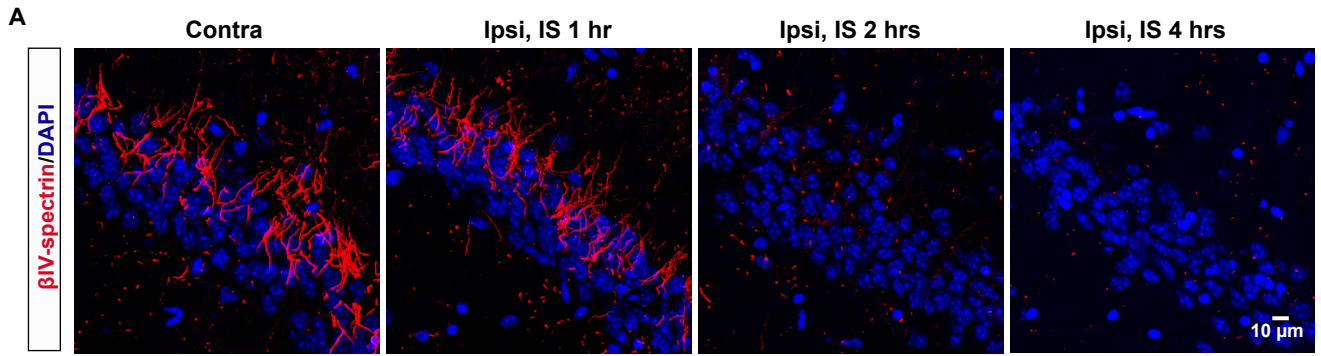
Figure S2. AIS cytoskeleton is rapidly disrupted after injury, related to Figure 1. (A) βIV-spectrin is completely disrupted after 2 hrs MCAO. (B) Quantification of the normalized F.I. of βIV-spectrin immunostaining from the CA1 pyramidal neurons after various times of MCAO. (C, D) Immunofluorescent staining of CA1 regions and immunoblot of hippocampal tissue homogenates with an AnkG antibody against the spectrin binding domain show disruption of AnkG after 2 hrs MCAO. P values in (B) are determined using One-Way ANOVA with *post hoc* Bonferroni's multiple comparisons test. N represents the number of mice analyzed. Data are presented as mean ± SEM.

A

Ky7.2/DAPI

Contra | Ipsi, IS 1 hr

Ipsi, IS 2 hrs | Ipsi, IS 4 hrs

10 μm

B

Normalized F.I. of K$_V$7.2

P = 0.007

P = 0.021

IS 1 hr | IS 2 hrs | IS 4 hrs

3 | 3 | 3

C

βIV-spectrin

Contra

Ipsi
IS 1 hr

1 μm

Intensity

0   0.5   1.0   1.5   2.0   2.5

Distance (μm)
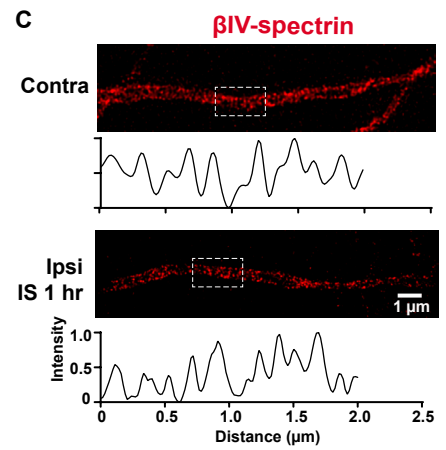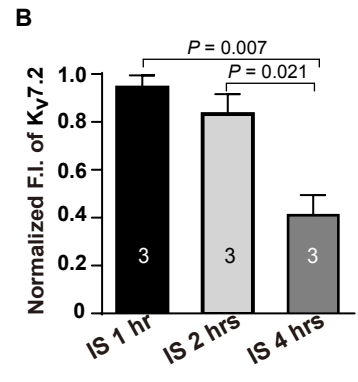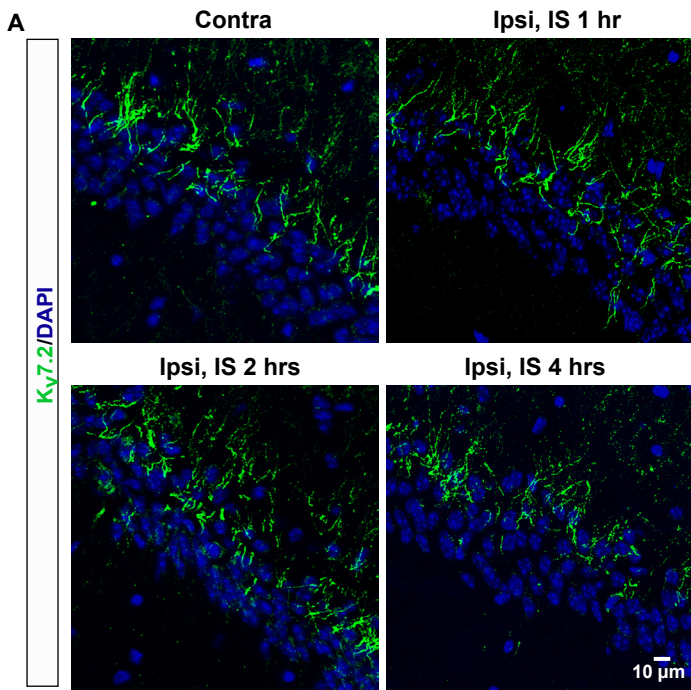
Figure S3. K$_v$7.2 is resistant to injury-induced disruption, related to Figure 2. (A, B) Representative images and quantification indicate that K$_v$7.2 mostly preserves at the AIS after injury. The ipsilateral F.I. was normalized to the contralateral from the same mouse. (C) STED superresolution images of βIV-spectrin immunostaining show periodic distribution at the AIS of hippocampal CA1 pyramidal neurons after 1 hr MCAO. Boxes indicate analyzed areas showed below. P values in (B) are determined using One-Way ANOVA with *post hoc* Bonferroni's multiple comparisons test. N represents the number of mice analyzed. Data are presented as mean ± SEM.

A

NF-186 sgRNA   1   1   2   2   3   3   4   4
Cas9   +   −   +   −   +   −   +   −
T7E1   Marker +   +   +   +   +   +   +   +

F_{cut} 33   39   61   24

B

NF-186 sgRNA   Pan-Nfasc   Cas9/merged

AAV non-infected region

AAV infected region

10 µm

C

NF-186 intensity ratio

P = 0.0009

Cas9

Cas9 + NF-186 sgRNA

D

AnkG   NF-186 sgRNA   Cas9/Merged

Contra

IS 2 hrs, Ipsi

10 µm
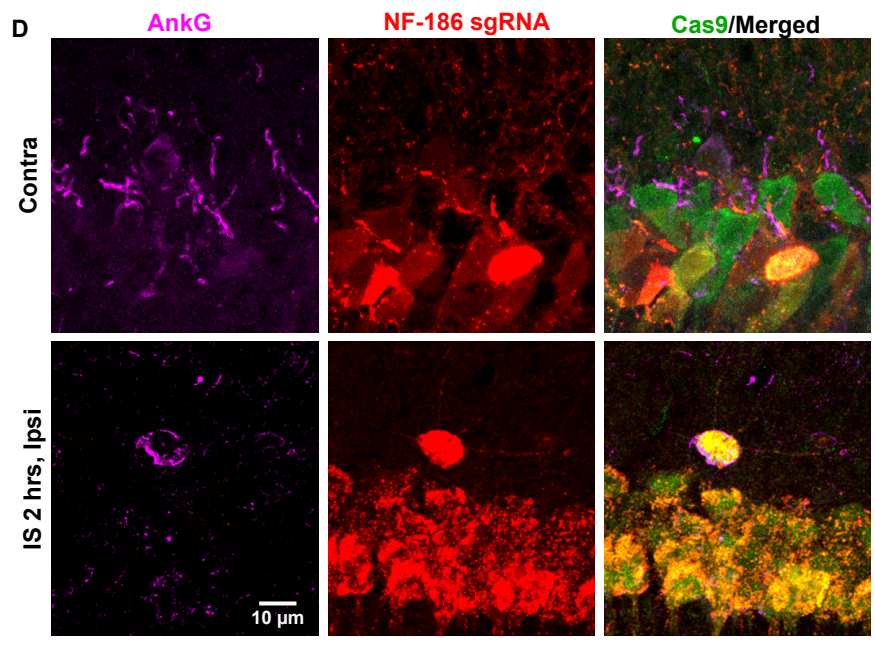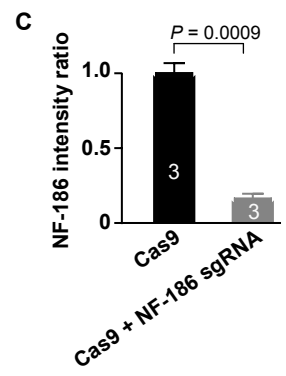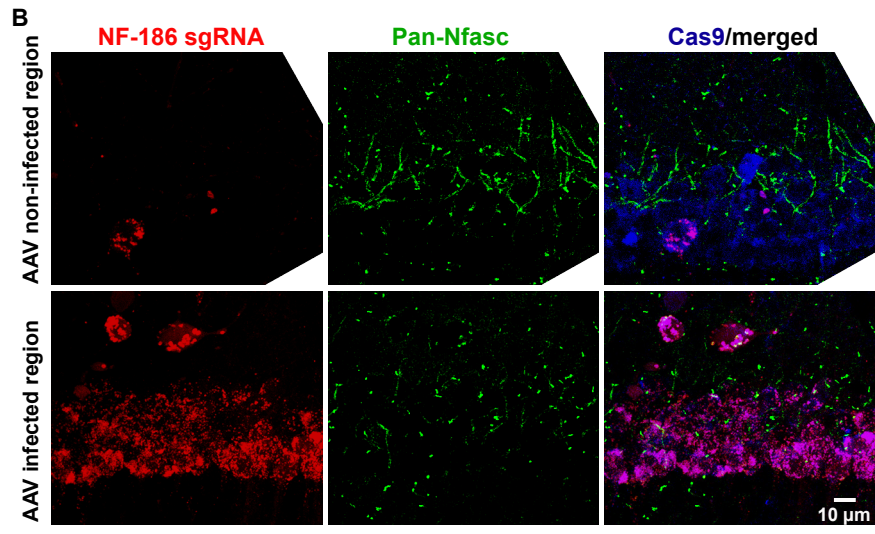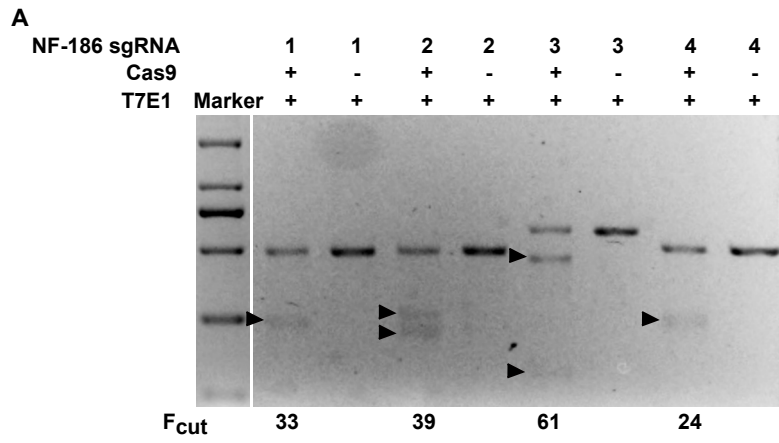
Figure S4. The efficiency of NF-186 sgRNA-directed CRISPR/Cas9 genome editing *in vitro* and *in vivo*, related to Figure 5. (A) The cleavage efficiency of four sgRNAs targeting NF-186 in the N2A cell *in vitro*. The sgRNA-3 is highly efficient for Cas9 to cleave NF-186. F_{cut} value is calculated as the percentage that total density of NF-186 is divided by the density of cleaved bands. Arrow heads indicate cleaved bands. (B) Representative confocal images of Nfasc immunostaining in the hippocampal CA1 region of Emx1-Cre-dependent Cas9 expressing mice 7 weeks after delivery of AAVs containing NF-186 sgRNA-3. (C) Quantification shows a significant reduction of Nfasc intensity in the CA1 region infected with AAVs compared to without AAVs 7 weeks after virus delivery in the absence of MCAO. (D) Representative images show that AnkG staining preserves 7 weeks after sgRNA AAV infection, but is completely disrupted after injury. P value in (C) is determined using unpaired t-test. N denotes the number of mice analyzed. Data are presented as mean ± SEM.
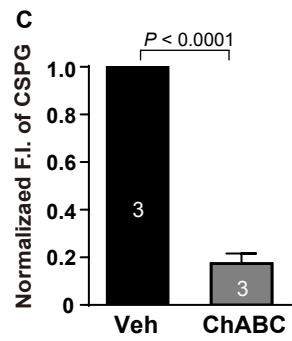
A

ChABC (20 U/ml) → MCAO Surgery → Sacrifice (Immunostaining)

-72 hrs | 0 | 2 hrs

B CSPG — DAPI/Overlay (Veh, ChABC) 10 µm

C

Normalizaed F.I. of CSPG

$P < 0.0001$

Veh — ChABC

D Nfasc — $Na_V1.6$ — DAPI/Overlay (Veh, ChABC) 30 µm

E

Normalizaed F.I. of Nfasc

Veh — ChABC

F

Normalizaed F.I. of $Na_V1.6$

Veh — ChABC

G $Na_V1.6$ — Pan-Nfasc — DAPI/Overlay

Ipsi, IS 2 hrs, Veh

Ipsi, IS 2 hrs, ChABC (20 U/ml) 10 µm
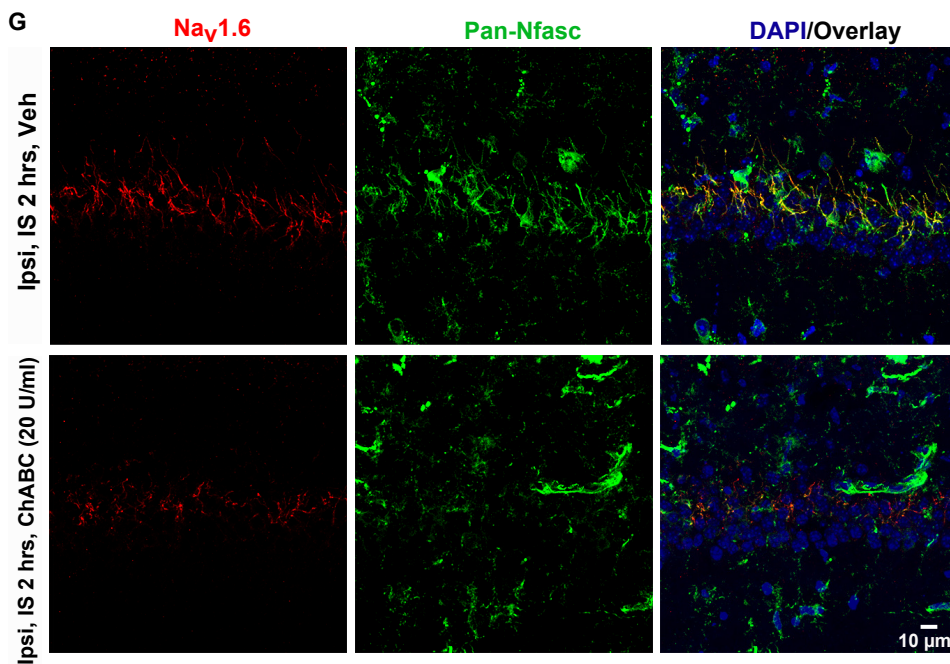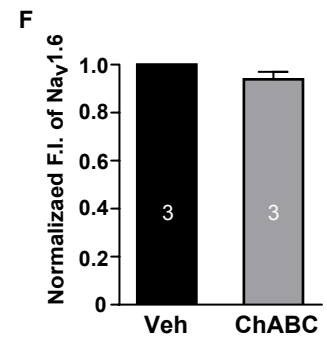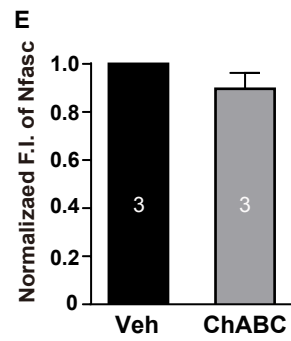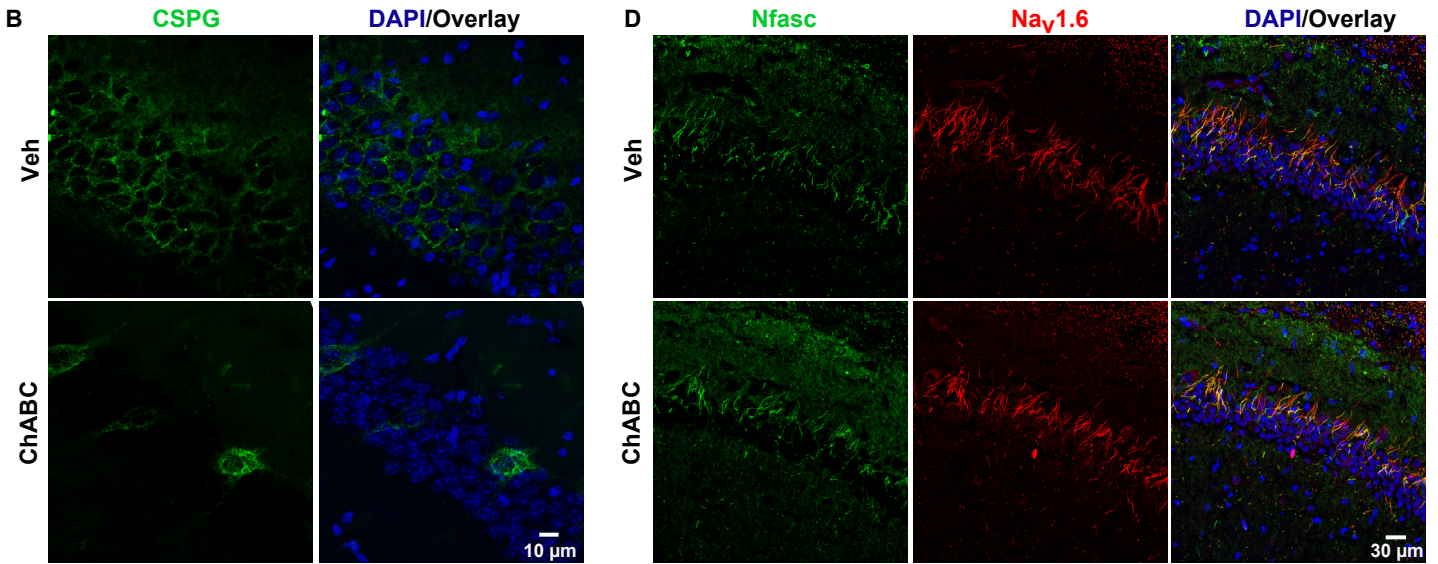
Figure S5. Depletion of ECM promotes $Na_v1.6$ disruption after injury, related to Figure 5. (A) Schematic of the experimental paradigm for ChABC delivery and MCAO surgery. ChABC (20 U/ml) was delivered into the hippocampal CA1 region 72 hrs before MCAO surgery. (B, C) CSPG is mostly disrupted 72 hrs after ChABC delivery in the absence of MCAO injury. (D–F) ChABC administration alone has no effect on the clustering of Nfasc and $Na_v1.6$ in hippocampal CA1 pyramidal neurons in the absence of MCAO injury. The ipsilateral ChABC F.I. was normalized to the contralateral Veh from the same mouse. (G) Representative confocal images show a dramatic reduction of $Na_v1.6$ immunostaining in hippocampal CA1 pyramidal neurons of 2 hrs MCAO mice treated with ChABC compared to Veh.

A

MCAO Surgery
CsA (20 mg/kg)

Sacrifice
(Immunostaining)

|————————————|————————————————————|——————————|
0 hr   2 hrs

B

| | AnkG | Na$_V$1.6 | DAPI/Overlay |

Contra

Ipsi

30 um

C
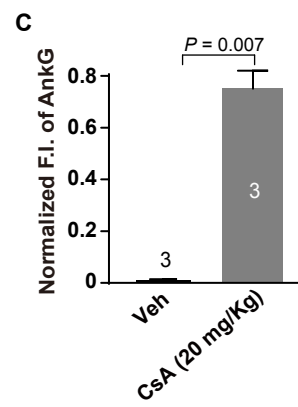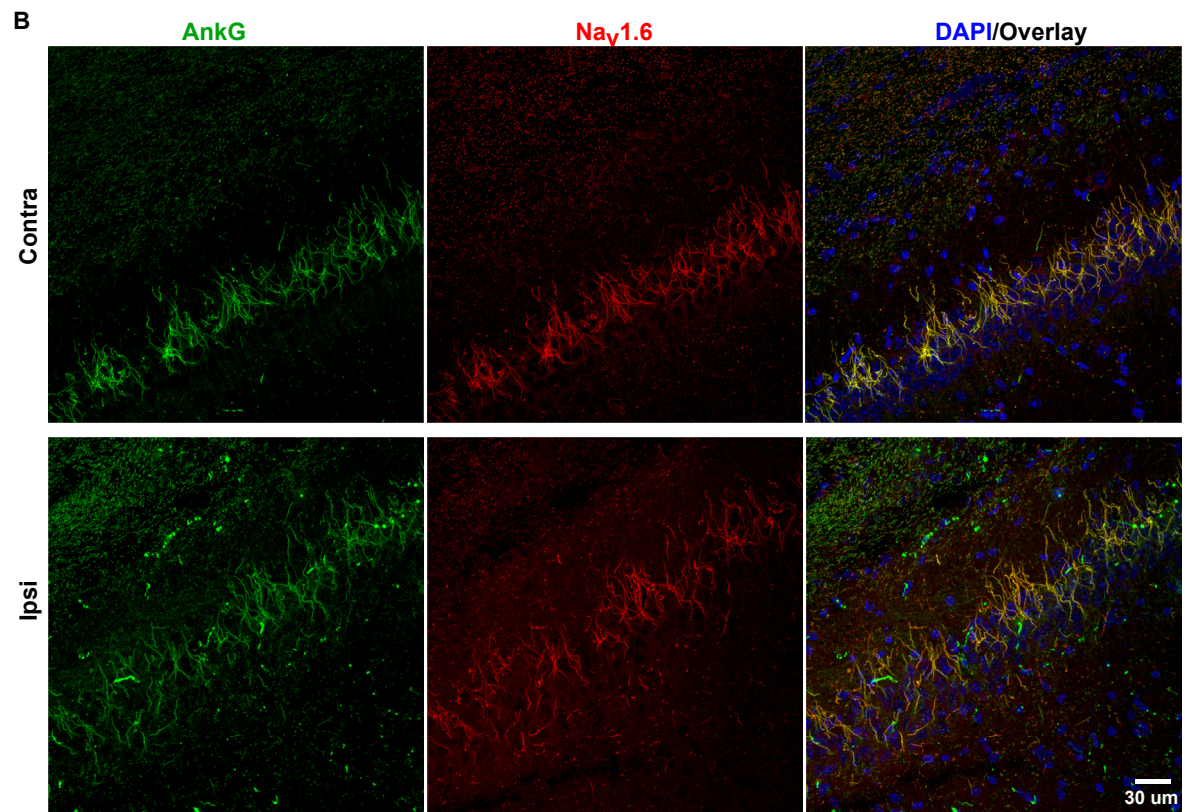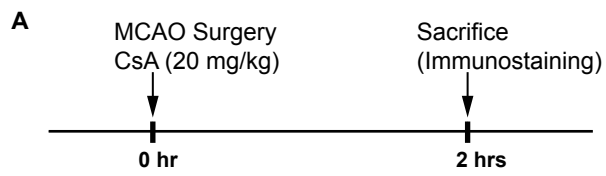
Figure S6. Inhibition of calcineurin with CsA prevents disruption of AnkG after injury, related to Figure 6. (A) Schematic of the experimental paradigm for Cyclosporine A (CsA) delivery and MCAO surgery. CsA (20 mg/kg) was administered by an intravenous injection immediately after MCAO surgery. (B) Representative confocal images of $Na_v1.6$ and AnkG immunostaining of the ipsilateral and contralateral hippocampal CA1 regions from a 2 hrs MCAO mouse treated with CsA. (C) Quantification shows that administration of CsA largely prevents disruption of AnkG induced by injury. The ipsilateral F.I. was normalized to the contralateral from the same mouse. P value is determined using unpaired t-test. N indicates the number of mice. Data are presented as mean ± SEM.

A

	Contra Veh	Ipsi, IS 2 hrs Veh	Ipsi, IS 2 hrs 30 mg/kg MDL28170	Ipsi, IS 2 hrs 60 mg/kg MDL28170

B
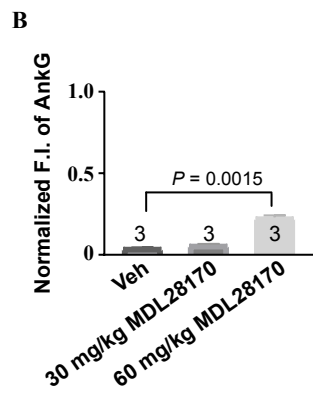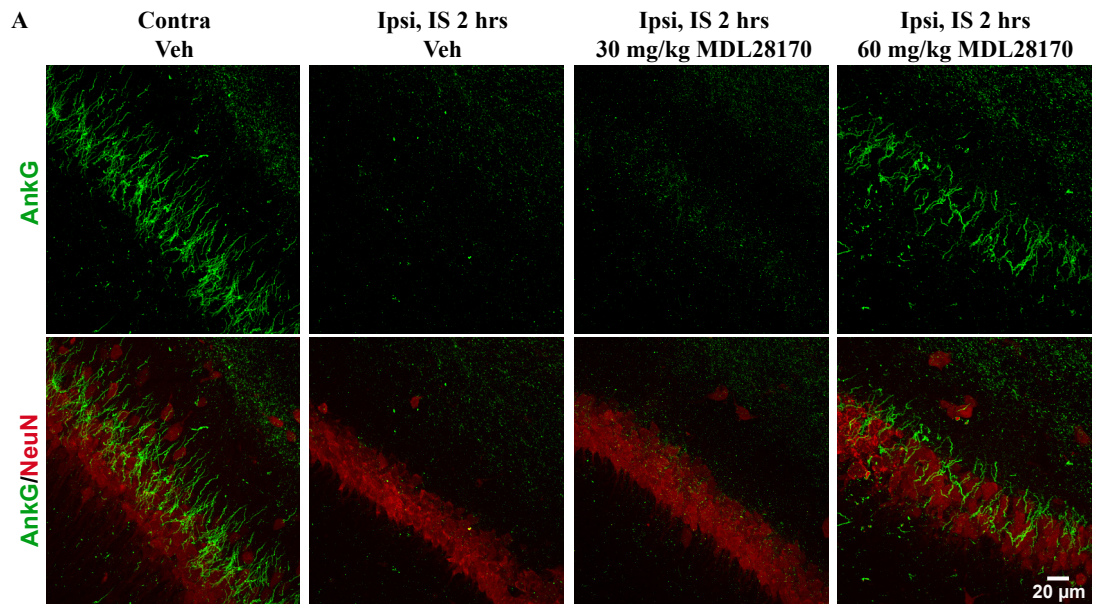
Figure S7. Inhibition of calpain attenuates disruption of the AIS cytoskeleton after injury, related to Figure 6. (A, B) Representative confocal images (*A*) and quantification (*B*) of AnkG (green) immunostaining in the hippocampal CA1 region of MCAO treated with vehicle, 30 mg/kg MDL 28170 or 60 mg/kg MDL 28170. MDL 28170 were administered by an intravenous injection immediately after MCAO surgery. Treatment with 60 mg/kg MDL 28170 partially preserved AnkG at the AIS of hippocampal CA1 pyramidal neurons after injury. P value is determined using One-Way ANOVA with *post hoc* Bonferroni's multiple comparisons test. N indicates the number of mice analyzed. Data are presented as mean ± SEM.
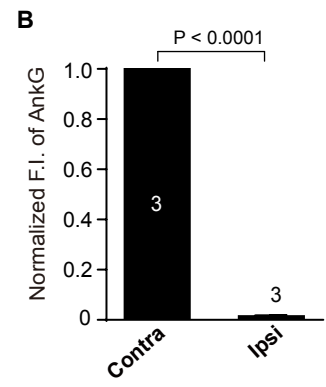
A

Contra
17-AAG

Ipsi, IS 2 hrs
17-AAG

AnkG/DAPI

20 μm

B

P < 0.0001

Normalized F.I. of AnkG

3

3

Contra   Ipsi

C

Contra

Ipsi, IS 2 hrs
50 mg/kg BBG

Ipsi, IS 2 hrs
2.5 mg/kg Nefidipine

AnkG/DAPI

20 μm
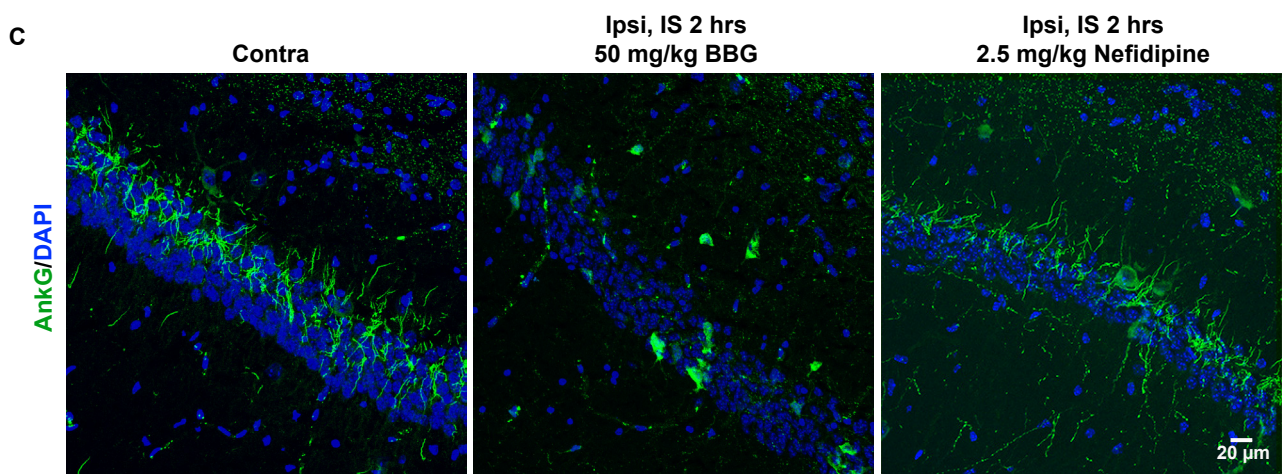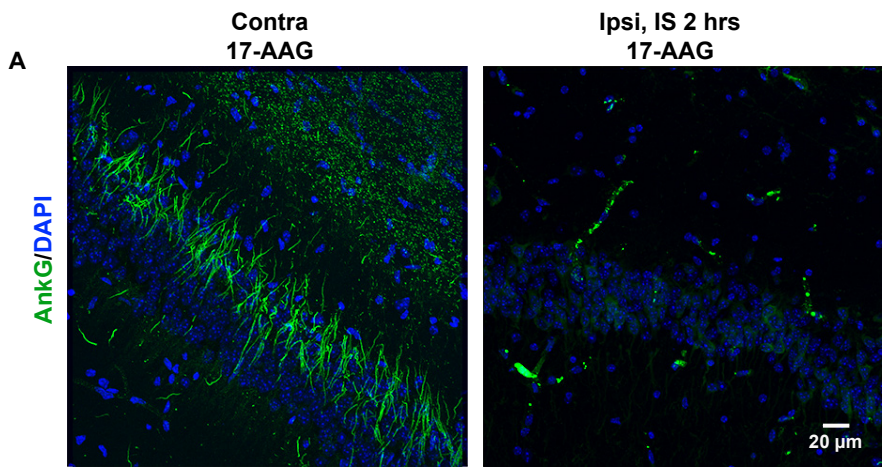
Figure S8. Blockade of L-type voltage-gated calcium channels, but not Hsp90, prevents AIS disruption after injury, related to Figure 6 and the discussion. (A, B) Hsp90 was inhibited with 17-(Allylamino)-17-demethoxygeldanamycin (17-AAG, 25 mg/kg) by an intravenous injection. The ipsilateral F.I. was normalized to the contralateral from the same mouse. P value is determined using paired t-test. (C) Inhibition of P2X7 with brilliant blue G (BBG, 50 mg/kg) by an intravenous injection has no effect on injury-induced AIS disruption. Nefidipine (2.5 mg/kg) was used to block L-type voltage-gated calcium channels by an intravenous injection.

A

Contra — Ipsi, IS 30 mins — Contra — Ipsi, IS 45 mins

AnkG

Na$_V$1.6/DAPI

50 um

Nfasc/DAPI

B

F.I. of AnkG

$P < 0.0001$ $P < 0.0001$

tMCAO 30 mins   tMCAO 45 mins

F.I. of Na$_V$1.6

$P = 0.044$

tMCAO 30 mins   tMCAO 45 mins

Normalized F.I. of Nfasc

Contra
Ipsi

tMCAO 30 mins

C

Training → Probe

Day 1   Day 2   Day 3   Day 4   Day 5   Day 6

Sham + Veh

tMCAO + Veh

tMCAO + FK506

D

Spatial training

- - Sham + Veh (n=10)
- □ tMCAO + Veh (n=10)
- ▽ tMCAO + FK506 (n=10)

Swimming speed (cm/sec)

Spatial Training Days

E

Swimming Speed (cm/sec)

Sham   tMCAO + Veh   tMCAO + FK506

Figure S9. Transient MCAO for behavioral tests, related to Figure 7. (A) Representative confocal images of AnkG, Na$_v$1.6 and Nfasc in the hippocampal CA1 regions of mice subjected to 30 mins or 45 mins *t*MCAO followed by 4 days reperfusion. (B) Quantification of the normalized F.I. of AnkG, Na$_v$1.6 and Nfasc corresponding to (A). The ipsilateral F.I. was normalized to the contralateral from the same mouse. (C) Representative track plots of three groups of mice: sham + Veh, *t*MCAO (30 minutes MCAO following by reperfusion of 4 days) + Veh or *t*MCAO + FK506 (2.5 mg/kg) during the training days and on the probing day 6. (D, E) Quantifications of the swimming speed during the training days and probe day show no difference among three groups of mice. P values in (B) are determined using paired t-test. N indicates the number of mice analyzed. Data are presented as mean ± SEM.
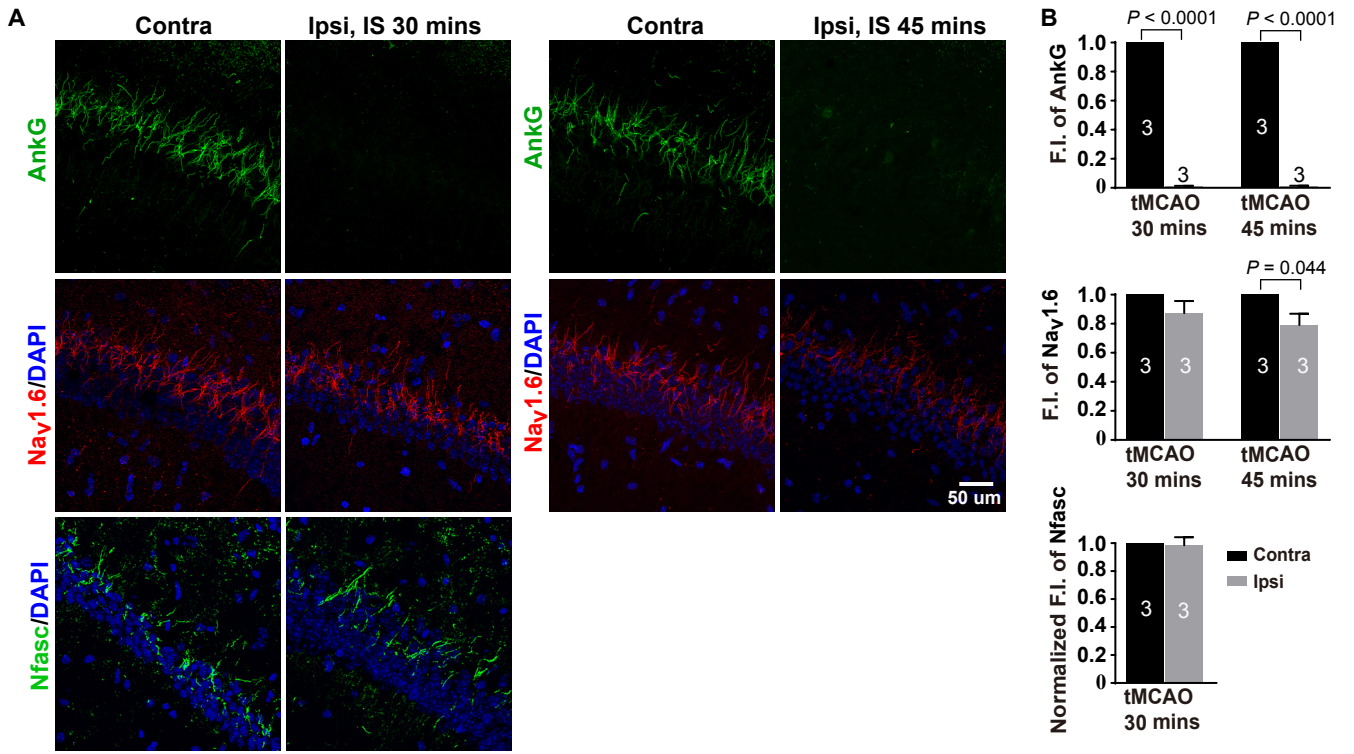
Table S1. Primary antibody sheet, related to Figures 1, 2, 5 and 6, and the transparent methods.

Name	Dilution	Host	Brand	Catalog Number
Anti-Na$_v$1.6 (SCN8A)	1:200	Rabbit	Alomone	ASC-009
Anti-NeuN antibody	1:1000	Rabbit	ABCam	Ab177487
Anti-Ankyrin G	1:200	Mouse	NeuroMab	N106/36
Ankyrin G (463)	1:200	Mouse	Santa Cruz	sc-12719
Anti-Neurofascin	1:200	Chicken	R&D Systems	AF3235
Anti- mCherry Monoclonal	1:1000	Rat	Invitrogen	M11217
Anti-GFP	1:1000	Chicken	Aves Labs	GFP-1020
Anti-GFP Polyclonal	1:1000	Rabbit	Invitrogen	A11122
Anti-K$_v$7.2	1:200	Rabbit	Synaptic Systems	368103
Anti-βIV-spectrin	1:200	Rabbit	A gift from Matthew N. Rasband	

Transparent Methods

Animals

Adult male ICR mice, initially weighing 27-30 g (age 56 days approximately), were used for middle cerebral artery occlusion (MCAO) surgery. Cre-dependent CRISPR-Cas9 knock-in C57BL/6 mice (a kind gift from Dr. Tian Chi, The Jackson Laboratory Stock No: 024857) were crossed with Emx1-Cre knock-in C57BL/6 mice (a kind gift from Dr. Ke Tang, Mouse Genome Informatics ID: 1928281) to generate an Emx1-cre/Cas9 mouse line. All mice were maintained under standard housing conditions of 22 ± 2℃, 50 ± 10% relative humidity and a 12 hours (hrs) light/dark cycle, and food and water were available *ad libitum*. All experiments were conducted in accordance with animal protocols approved by the Institutional Animal Care and Use Committees of ShanghaiTech University, China.

MCAO Surgery

Animal models of focal cerebral ischemia were achieved by occlusion of the middle cerebral artery (MCA) to represent ischemic brain damage observed in human patients suffering from stroke. MCAO surgery was performed as previously described (Longa et al., 1989). Briefly, body temperature was maintained at 37 ± 0.5℃ using a homoeothermic heating pad throughout the surgery. Cortical blood flow was measured with a laser Doppler flow meter (LDF) (VMS-LDF1; Moor Instruments, Axminster, UK). The right external carotid artery was transected slight on the anterior surface, and a silicone-coated nylon monofilament (0.25 mm ± 0.02 tip) was advanced through the common carotid artery into the branch point of the MCA from the internal carotid artery (LDF dropped to < 20 % of baseline). The nylon filament remained in the MCA for various times, and then animals were sacrificed for analyses at various times of post-occlusion (1 hr, 2 hrs, 4 hrs, and 6 hrs). For transient MCAO (*t*MCAO), nylon filament was withdrawn 30 minutes (mins) after occlusion to restore the blood flow in the MCA by >70% of baseline measured by LDF. Sham animals were subjected to the same surgical procedure without occlusion of the MCA. Animals began to perform behavior tests at 4 days after the onset of 30 mins occlusion. Intra-ischemic neurologic deficit was confirmed and scored as follows: 0, no deficit; 1, forelimb weakness and torso turning to the ipsilateral side when held by tail; 2, circling to affected side; 3, unable to bear weight on affected side; and 4, no spontaneous locomotor activity or barrel rolling. Animal performed no deficit was removed from further study. Infarction was assessed using the triphenyl-tetrazolium chloride (TTC) staining method.

Drug Administration

ChABC (20 U/ml) was delivered into the hippocampal CA1 region 72 hrs prior to MCAO surgery. For behavioral tests, mice that were subjected to *t*MCAO received a dose of FK506 (5 mg/kg) immediately after surgery and another 3 doses (2.5 mg/kg) in the following 3 days (1 dose/day) by an intravenous (IV) injection till behavioral tests. All other drugs (1 dose) were administered via an IV injection immediately after surgery.

Immunostaining and TUNEL staining

For tissue preparations, anesthetized mice were transcardially perfused with 0.9% saline followed by paraformaldehyde (PFA) in 0.1 M phosphate buffered saline (PBS), pH 7.4 (1%

PFA for AnkG or Na$_v$1.6 staining and 4% PFA for Nfasc). Brains were dissected and post-fixed for 4 hrs (for AnkG or Na$_v$1.6 staining) and overnight (for Nfasc staining) correspondingly at 4℃, and then transferred to 20% sucrose in 0.1 M PBS at 4℃ for over 48 hrs. Finally, coronal cryostat sections (25 μm) were obtained using a microtome and mounted on the slides.

For immunostaining, slices were blocked in 10% normal goat serum 0.1 M PB containing 0.3% TX-100 (PBTGS), then incubated overnight at 4℃ with primary antibodies (diluted in PBTGS). The primary antibodies used in this study were: mouse anti-AnkG (1:200; N106/36, NeuroMab), Rabbit anti-Na$_v$1.6 (1:200; ASC009, Alomone), Mouse anti-AnkG (1:200, Santa Cruz), Chicken anti-Nfasc (1:400; AF3235, R&D Systems), Rabbit anti-GFP (1:1000, Aves Lab), Rat anti-mCherry (1:1000, Invitrogen), Rabbit anti-NeuN (1:1000, ABCam), Rabbit anti-K$_v$7.2 (1:200, Synaptic Synapses), Rabbit anti-βIV-spectrin (1:200, a gift from Matthew N. Rasband). After three washes with PBTGS, sections were incubated for 2 hrs at room temperature with corresponding secondary antibodies (Life Technologies). The terminal deoxynucleotidyl transferase–mediated deoxyuridine triphosphate nick-end labeling (TUNEL) assay was performed according to the manufacturer's instructions (Promega). Finally, slides were stained nuclei with DAPI (Sigma) and coverslipped with the anti-fade mounting medium.

Electrophysiological recordings

Adult mice subjected to MCAO or sham were anesthetized by isoflurane and transcardially perfused with ice-cold ACSF. Adult brains slices for electrophysiological recordings were prepared as previously described (Jiang et al., 2015; Yu et al., 2012). Briefly, mice were decapitated. Brains were removed, and quickly transferred to ice-cold modified ASCF containing: 93 mM NMDG, 93 mM HCl, 2.5 mM KCl, 1.2 mM NaH$_2$PO$_4$, 30 mM NaHCO$_3$, 20 mM HEPES, 25 mM glucose, 5 mM sodium ascorbate, 2 mM Thiourea, 3 mM sodium pyruvate, 10 mM MgSO$_4$ and 0.5 mM CaCl$_2$ with PH 7.35. Mouse brains were sectioned 350 μm coronal slices by vibratome at a speed of 0.03 mm/s, and transferred to 37℃ NMDG solution for recovery 15 mins and then incubated in 37℃ ACSF solution consisting of 126 mM NaCl, 4.9 mM KCL, 1.2 mM KH$_2$PO4, 2.4 mM MgSO$_4$, 2.5 mM CaCl$_2$, 26 mM NaHCO$_3$, 20 mM Glucose for 1 hr. One brain slice was transferred in the chamber containing 30−32℃ ACSF. Whole cell configuration was achieved in the hippocampal CA1 pyramidal neurons with an upright microscope (BX51WI, Olympus) equipped with a 60× objective (water-immersion, NA 1.00) and differential interference contrast (DIC). Recording pipettes (10−12 MΩ) were fabricated using a P1000 micropipette puller (Sutter Instrument, USA) and filled with an internal solution containing: 136 mM K-gluconate, 6 mM KCl, 1 mM EGTA, 2.5 Na$_2$ATP, 10 mM HEPES (280 mOsm, pH=7.2 with KOH). Recordings were collected with a low-pass filter at 2 kHz using Multiclamp 700B and Digidata 1322A/D converter, and sampled at 10 kHz using pCLAMP software. Recordings were discarded if series resistance was >40 MΩ or varied >15% or resting membrane potential is positive than -50 mV. Action potential properties were analyzed from the first action potential elicited using CLAMPFIT software. Action potential threshold was documented as the voltage of the first point where the dV/dt reaches 10 V/s during the rate-of-rise phase of the phase-plane plot of the membrane voltage against its change rate (Evans et al., 2015). Action potential amplitude was determined as the difference between the peak point and the threshold. Spontaneous and miniature postsynaptic currents (sPSCs and mPSCs) were analyzed using MiniAnalysis software (Synaptosoft, USA). Detection threshold was 8 pA.

Confocal imaging

To compare AIS length and fluorescence intensity between ipsilateral and contralateral, images were acquired on the confocal microscope Nikon Ti-E+A1 R SI fitted with an Axiocam digital camera and taken using 40X (1.0 NA) objective, digitized in z-stacks of 0.2–0.5 μm thick optical sections. Neurons in regions of interest were imaged with 40X lens.

The length and fluorescence intensity of AnkG and $Na_v1.6$ immunostaining along the AIS was determined using Image J (NIH)-Fuji. For the somatosensory cortex and the thalamus, AISs that were located at 4 corners and 1 middle were chosen for analyses. Total 60 AISs from three images (20 AISs/image from 5 locations) were averaged for each mouse. For calculation of the AIS length in the hippocampus, AISs that were located in the middle and the two sides were chosen for analysis and total 45 AISs from three images (15 AISs/image from 3 locations) were averaged for each mouse.

For the fluorescence intensity of hippocampal AISs, the integrated intensity was calculated at the area encompassing all AISs of the hippocampal CA1 pyramidal cells in an image unless otherwise stated. For the integrated intensity of individual hippocampal AISs, the AIS that could be distinguished from other AISs were analyzed to determine effect of Cas9-dependent knockdown of NF-186 on injury-induced AIS disruption *in vivo*. Layers at the Z axis were manually selected to be merged for displaying the integrity of individual AISs.

The start and end of the AnkG or $Na_v1.6$-positive AIS was defined as the point at which the immunoreactivity fell below 10% of the maximum fluorescence intensity along the AIS (>10 μm in length generally) (Ko et al., 2016; Schafer et al., 2009). Integrated intensity of immunofluorescence was calculated at individual AIS area surrounding the start point and the end point for the somatosensory cortex and the thalamus as described previously (Grubb and Burrone, 2010) or at the area encompassing all AISs in an image for the hippocampus.

STED

Stimulated emission depletion (STED) was used to investigate whether the molecular ultrastructure of $Na_v1.6$ at the AIS was changed after ischemic injury. STED images were obtained by using the Leica TCS SP8 STED 3X microscope, equipped with white light pulse laser (WLL2), STED laser (592 nm, 660 nm), oil immersion 100x / NA 1.4 objective lens (HC PL APO CS2, Leica) and TCS SP8 time-gated system. The STED depletion laser was co-aligned with the excitation laser, and selectively deactivated the excited fluorophores surrounding the focal point, which allows an increased resolution of 30–40 nm obtained by shrinking point-spread function (PSF) of the microscope. Images were acquired in both confocal mode and STED mode with 1024 x 1024 formats. Acquisition settings such as laser power, image size, pixel dwell times, line average, frame accumulation and time-gating interval (1–6 ns post-pulse time window) were optimized for achieving the best imaging quality. Deconvolution of STED images was performed by Huygens software (Scientific Volume Imaging) with the Huygens classical maximum likelihood estimation (CMLE) deconvolution algorithm.

Image processing and analysis: All Images were exported from LAS X (Leica Microsystems), and further processed by Fiji software (National Institutes of Health). Brightness and contrast on entire images were linearly adjusted. For quantitatively analyzing the distance

and distribution pattern of Na$_v$1.6 in neurons, lines across the structures were drawn, the intensity profiles were measured by Fiji or LAS X, All the intensity and distance data were plotted using Graphpad prism software (Graphpad Software, Inc.), and all figures were composed using Illustrator software (Adobe Systems, Inc.).

Immunoblotting

For immunoblotting, mice were anesthetized, decapitated and brains were removed quickly. The hippocampi were dissected into ipsilateral (stroke side) and contralateral sides, and then were flash-frozen in liquid nitrogen, and transferred into -80℃ to be stored till homogenization. Protein was separated by SDS-PAGE (Bis-Tris, 4-12% gradient gels) and then transferred to nitrocellulose membrane at 100 mA for 22 hrs in 4℃. Membranes were blocked for 2 hrs with 5% BSA and incubated with primary antibodies followed by incubation with the appropriate horseradish peroxidase-conjugated secondary antibodies. The primary antibodies used were: mouse anti-AnkG (1:500; N106/36, NeuroMab), Rabbit anti-Na$_v$1.6 (1:200; ASC009, Alomone), chicken anti-Nfasc (1:500; cat no. AF3235, R&D Systems). ECL detection kit (Bio-Rad) was used for signal detection. Data were analyzed using ImageJ (NIH)-Fuji software.

AAV viruses and Intravitreal injection.

Synthetic single-guide RNAs (sgRNAs) targeting Nfasc were designed using the CRISPR tool (http://crispr.mit.edu) to minimize potential off-target effects. The target sequences are listed as follows:

sgRNA-1, 5'-gtgggctgggcagcggggagcagg-3';

sgRNA-2, 5'-ggtgatcgacttccgcagtggtggtgg-3';

sgRNA-3, 5'-gcaaggaagcaacctggatggcgg-3';

sgRNA-4, 5'-gaaccaaactgggaaagcagatgg-3'.

The efficacy of sgRNA was assessed by F$_{cut}$ in the Neuro2A (N2A) cell lines *in vitro*, and the most efficient sgRNA was selected to be constructed into AAV1/2 vectors packaged into AAV1/2 viruses in 293T cells. As a control, the scrambled sgRNA sequence that was designed to target lacZ gene from Escherichia coli is listed as follows as previously described: TGCGAATACGCCCACGCGATGGG (Swiech et al., 2015). For NFAT-EGFP AAVs, NFAT-EGFP (a kind gift from Dr. Antos Christopher) was cloned into the AAV vector. For virus delivery, deeply anesthetized mice were fixed in a stereotaxic apparatus, and AAV1/2 Nfasc-sgRNA viruses were injected into the right hemisphere of the hippocampus CA1 at 0.18 cm posterior to the bregma, and 0.1 cm lateral to the midline with 0.15 cm from the surface (Paxinos et al., 2001), while AAV2-GFP viruses were delivered into the contralateral hemisphere. Seven weeks following the AAV injection, mice were subjected into 2 hrs occlusion at the ipsilateral sides of Nfasc-sgRNA AAV injection and then prepared to immunostaining.

Morris water maze (MWM)

Mice were tested in MWM to monitor their spatial learning and memory. The water maze consisted of a pool (120 cm in diameter and 50 cm in height) that was painted black and filled with water containing black nontoxic paint with the temperature at 23 ± 1℃. The pool was divided into four quadrants named as target quadrant (TA), adjacent left quadrant (AL), adjacent right quadrant (AR) and opposite quadrant (OP), respectively. The water in the tank was stirred

in between animal trials to disrupt odor trails. The room was furnished with several extra-maze cues immobile throughout the entire experiment process. The animal's movement was recorded and analyzed using a computerized video-tracking system (Ethovision@3, Noldus Information Technology, Wageningen, Netherlands).

In the spatial reference memory test, from the fourth day to eighth day post-*t*MCAO treatments, a movable black circular platform (10 cm in diameter) was located in the center of TA and submerged 1 cm below the water surface. Mice were trained to find the hidden platform with the extra-maze cues to examine acquisition of spatial reference memory. Mice were trained once a day for 5 consecutive days (day 1 to day 5) and each training consisted of four trials. In each trial, mice were placed into the pool, facing the wall at each of the four quadrant edges, randomly chosen across trials. If mice found the platform within 60 seconds, they were allowed to stay in the platform for 15 seconds. Otherwise, the experimenter guided the mouse to the platform and allowed it to rest for 15 seconds. Mice were then returned to a holding cage for 60 mins before the next trial. The parameters were recorded: swimming speed; escape latency, swimming time to locate the hidden platform.

In the probe test (day 6), 24 hrs after the last trial of training, the platform was removed to assess the mouse's memory of the platform position. Mice were tested once with a single trial of 60 s. The parameters were recorded: swimming speed; quadrant time, exploring time in each quadrant of the pool; platform crossing, the number of crossings at the place where the platform was located during training.

Novel object recognition (NOR)

The object recognition test was performed as previously described (Zhao et al., 2013). Briefly, mice were placed in a square box with an open top, painted black, 100 cm wide ×45 cm tall. The arena was dimly illuminated and surrounded by a black curtain to minimize effects of environment on behavior tests. In session 1 (S1), animals were placed in the empty open field for 5 mins. This first session served as a familiarization stage to prevent anxiety and to assess locomotor activity. Twenty four hrs after S1, in sessions 2 (S2), animals were exposed to a parallel configuration of two same objects 1 and 2 in the field S1 performed for 10 mins, then rested in cages for 2 hrs. In session 3 (S3), object 1 was replaced by a novel object, object 3, to test recognition ability of the new object for 10 mins. All objects were located at the same distance from the wall of the field, and the field and objects were cleaned with 70% (vol/vol) ethanol and dried after every session. Each session was recorded by a video camera suspended above the field and interfaced with a computerized tracking system using Ethovision@3 software (Noldus Information Technology, Wageningen, Netherlands). For S2 and S3, the duration of contacts with each object was calculated. A contact was defined as any time the mouse touched its nose or hands on the object to actively explore it, not just as a passing sniff as it passed by the object while walking around the field.

Statistics

Data were analyzed blindly to the experimental groupings by investigators. Statistical analyses and data plots were conducted by the GraphPad Prism 5.0 software (Graphpad Software, Inc.). Data were tested for significance using paired/unpaired t-test or one-way /two-

way ANOVA with *post-hoc* Bonferroni's multiple comparisons test, and P < 0.05 was considered significant. All figures were composed using Illustrator software (Adobe Systems, Inc.).

Supplemental References

Evans, M.D., Dumitrescu, A.S., Kruijssen, D.L.H., Taylor, S.E., and Grubb, M.S. (2015). Rapid Modulation of Axon Initial Segment Length Influences Repetitive Spike Firing. Cell Rep *13*, 1233-1245.

Grubb, M.S., and Burrone, J. (2010). Activity-dependent relocation of the axon initial segment fine-tunes neuronal excitability. Nature *465*, 1070-1074.

Jiang, X., Shen, S., Cadwell, C.R., Berens, P., Sinz, F., Ecker, A.S., Patel, S., and Tolias, A.S. (2015). Principles of connectivity among morphologically defined cell types in adult neocortex. Science *350*, aac9462.

Ko, K.W., Rasband, M.N., Meseguer, V., Kramer, R.H., and Golding, N.L. (2016). Serotonin modulates spike probability in the axon initial segment through HCN channels. Nat Neurosci *19*, 826-834.

Longa, E.Z., Weinstein, P.R., Carlson, S., and Cummins, R. (1989). Reversible middle cerebral artery occlusion without craniectomy in rats. Stroke *20*, 84-91.

Paxinos, G., Franklin, K.B.J., and Editors (2001). The mouse brain in sterostatic coordinates. San Diego: Academic Press: 2nd edition.

Schafer, D.P., Jha, S., Liu, F., Akella, T., McCullough, L.D., and Rasband, M.N. (2009). Disruption of the axon initial segment cytoskeleton is a new mechanism for neuronal injury. J Neurosci *29*, 13242-13254.

Swiech, L., Heidenreich, M., Banerjee, A., Habib, N., Li, Y., Trombetta, J., Sur, M., and Zhang, F. (2015). In vivo interrogation of gene function in the mammalian brain using CRISPR-Cas9. Nat Biotechnol *33*, 102-106.

Yu, Y.C., He, S., Chen, S., Fu, Y., Brown, K.N., Yao, X.H., Ma, J., Gao, K.P., Sosinsky, G.E., Huang, K.*, et al.* (2012). Preferential electrical coupling regulates neocortical lineage-dependent microcircuit assembly. Nature *486*, 113-117.

Zhao, Y.N., Wang, F., Fan, Y.X., Ping, G.F., Yang, J.Y., and Wu, C.F. (2013). Activated microglia are implicated in cognitive deficits, neuronal death, and successful recovery following intermittent ethanol exposure. Behav Brain Res *236*, 270-282.